ABSTRACT

Title of Thesis: INTEGRATION OF STEAM REFORMING AND CATALYTIC COMBUSTION IN A SINGLE PLATE REACTOR

Fletcher Alexi Robbins, Master of Science, 2004

Thesis Directed by: Associate Professor Dr. Gregory Jackson
Department of Mechanical Engineering

A novel co-flow heat exchanger intended for volumetrically efficient hydrogen production and utilizing catalytic surface combustion to drive endothermic steam reforming occurring in adjacent channels has been investigated experimentally and numerically. A single plate reactor has been developed for studying the complex interactions between H_2 or CH_4 combustion over a supported Pd catalyst and CH_4 steam reforming over a supported Rh catalyst. Experiments have been conducted to determine a stable window of operation for the system and to observe the effects that inlet temperature, steam to carbon ratio, and reforming flow rates have on surface temperatures and reformate composition. The experiments have been used to validate a transient model of the dual channel reactor design employing distinctly different surface chemistries. Modeling results show that reforming can be sustained with adequate

conversion to maintain combustion catalyst temperatures within the range where activity of both catalysts is high.

INTEGRATION OF STEAM REFORMING AND CATALYTIC COMBUSTION IN A SINGLE PLATE REACTOR

by

Fletcher Alexi Robbins

Thesis submitted to the Faculty of the Graduate School of the
University of Maryland, College Park in partial fulfillment
of the requirements for the degree of
Master of Science
2004

Advisory Committee:

Associate Professor Gregory Jackson, Chair
Associate Professor Jungho Kim
Assistant Professor Bao Yang

Dedicated to

my parents Larry and Regina,

my brother Ian, and of course,

to my fiancé, Catherine.

Your support has meant so much.

ACKNOWLEDGEMENTS

It is my great pleasure to thank my thesis advisory committee:

Professor Gregory S. Jackson, my thesis advisor and mentor. You have provided an opportunity and appreciation for learning that I will always carry with me. I have felt fortunate to have studied under you these past few years and thank you for your patience in helping me complete this endeavor.

Professor Jungho Kim, instructor of my undergraduate heat transfer course. You have an uncommon ability to reach your students and I was privileged to have you as a teacher. Thank you for your thoughtful remarks regarding my thesis.

Professor Bao Yang. I had only met you briefly, but will hopefully have more contact in the future as we are both currently pursuing thermoelectrics. Thank you for reading my thesis and serving on my committee.

I would finally like to thank the other members of the Reacting Flow Lab with whom I've shared this experience: Huayang Zhu, Tom McGrath, Roxanne Sai, Doug Crane, Seyed Reihani, Joe Plaia, Jeff Kramer, Bahman Habibzadeh, Ben Becker, and Vaughan Thomas. I hope all of you have success in what you do.

TABLE OF CONTENTS

LIST OF TABLES

LIST OF FIGURES

NOMENCLATURE

a_{cat}	surface area of catalyst per volume of washcoat	1/cm
a_{ch}	geometric surface area of channel per volume of channel	1/cm
a_{wc}	geometric surface area of washcoat per volume of washcoat	1/cm
$\overline{C}_{Pk,b}$	molar specific heat capacity for k^{th} species in catalyst bulk	erg/gmol*K
$\overline{C}_{Pk,s}$	molar specific heat capacity for k^{th} species on catalyst surface	erg/gmol*K
$C_{Pk,g}, C_{Pk,gs}$	specific heat capacity for gas species k in channel and washcoat	erg/g*K
$C_{P,sub}, C_{P,wc}$	specific heat capacity for washcoat and reactor substrate	erg/g*K
$\overline{C_{P,s}}$	effective specific heat capacity for washcoat, including catalyst support, catalyst particles, and gas in washcoat	erg/g*K
d_{hyd}	hydraulic diameter of channel	cm
D_k	ordinary mixture-averaged diffusion coefficients of k^{th} species	cm^2/s
$h_{k,g}, h_{k,gs}$	specific enthalpy of the k^{th} species in the channel and in washcoat	erg/g
$h_{k,gm}$	average specific enthalpy of species k between channel and washcoat	erg/g
h_T	heat transfer coefficient between channel flow and washcoat	erg/cm^2K
h_K	mass transfer coefficient between channel flow and washcoat	g/cm^2K
$\Delta_R H^{\circ}_{298K}$	heat of reaction at standard conditions	kJ/mol
n_k	moles of k^{th} species	
Nu_T	Nusselt number for heat transfer between channel and washcoat	
$Nu_{T,i}$	Nusselt number constants for heat transfer correlations	

P_k , P_{tot}	partial pressure of kth species and total pressure	atm
P_{sat}	saturation pressure	atm
Sh_k	Sherwood number for mass transfer of species k between channel and washcoat	
$Sh_{k,i}$	Sherwood number constants for mass transfer correlation	
$\hat{s}_k$	molar production rate of kth species per unit surface area	gmol/cm^{2}s
S/C	steam to carbon ratio	
t	time	s
t_w	half the thickness of the washcoat and substrate combined	cm
T_g , T_s	temperature in the channel flow and washcoat	K
u_g	mean axial velocity in the channel flow	cm/s
V_g	average Stefan velocity from the channel flow to the washcoat	cm/s
v_{sub}	volume of substrate to volume of channel	
W_k	molecular weight of the kth species	gmol/g
W_g , W_{gs}	mean molecular weight of gas-phase mixture in channel and washcoat	gmol/g
W_{gm}	average mean molecular weight between channel and washcoat	gmol/g
x, z	axial distance	cm
x_k	non-dimensional distance for mass transfer correlations	
x_T	non-dimensional distance for heat transfer correlation	
X_k	mole fraction of kth species	
$Y_{k,g}$, $Y_{k,gs}$	mass fraction of gas phase species k in the channel and washcoat	

$Y_{k,gm}$	average mass fraction of gas species k between channel and washcoat	
$YV_{k,g}$	mass weighted diffusion velocity of species k from channel to washcoat	cm/s
Γ_{cat}	surface site density of the catalyst	gmol/cm^2
ε	porosity of catalytic washcoat	
λ_s	effective thermal conductivity of solid reactor substrate with washcoat	erg/cm*K
η_{H_2}	hydrogen selectivity	
ρ_g, ρ_{gs}	gas phase density in the channel flow and washcoat	g/cm^3
ρ_{gm}	average gas phase density between the channel flow and washcoat	g/cm^3
ρ_{wc}, ρ_{sub}	solid phase density of washcoat and reactor substrate	g/cm^3
θ_k	surface site fraction of the kth surface species	
Θ_k^T	thermal diffusion coefficient for the kth species	
σ_{cat}	dispersion of catalyst	
χ_k	conversion of the kth species	
$\dot{\omega}_k$	molar production rate of kth species from gas-phase reactions	gmol/cm^3*s

Chapter 1

Introduction to Combined Combustion and CH_4 Steam Reforming

1.1 STEAM REFORMING VS. PARTIAL OXIDATION

Due to the current lack of a pure hydrogen infrastructure, researchers are examining ways to extract hydrogen from more readily available and distributable hydrocarbon fuels. They seek a process that will generate a hydrogen rich effluent stream requiring minimal cleanup and that will maintain high system efficiencies. Steam reforming (SR) and partial oxidation (POX) are the two most promising pathways under investigation. Several fuels have been investigated, including gasoline, but methane (CH_4), which is the main component in natural gas, offers the highest hydrogen to carbon ratio at 4:1 (Ahmed et al. 2001; Brown 2001). The primary reactions for steam reforming methane are

$$CH_4 + 2H_2O \Leftrightarrow CO_2 + 4H_2, \qquad \Delta_R H^{\circ}_{298K} = 165 \ (kJ/mol) \tag{1.1}$$

$$CH_4 + H_2O \Leftrightarrow CO + 3H_2, \qquad \Delta_R H^{\circ}_{298K} = 206 \ (kJ/mol) \tag{1.2}$$

and for partial oxidation are

$$CH_4 + \frac{1}{2}O_2 \Leftrightarrow CO + 2H_2, \qquad \Delta_R H^{\circ}_{298K} = -36 \ (kJ/mol) \tag{1.3}$$

$$CH_4 + O_2 \Leftrightarrow CO_2 + 2H_2, \qquad \Delta_R H^{\circ}_{298K} = -319 \ (kJ/mol) \tag{1.4}$$

Clearly, the two principal pathways differ substantially. Due to its endothermic nature, steam reforming (SR) requires an additional heat source to sustain the reactions. Researchers cite this requirement as the prohibitive element to a pure SR system due to its consequences on system efficiency (Rosen 1991; Balasubramanian et al. 1999; Ahmed and Krumpelt 2001; Zhu et al. 2001). However, use of heat recovery systems can make steam reforming an attractive alternative for many H_2 generation applications. Partial oxidation has the advantage of being self sustaining, but it produces a substantially lower H_2 concentration in the effluent particularly when O_2 is supplied as air. The two processes differ in the maximum hydrogen concentration achievable in the effluent. Undiluted steam reforming of methane has been shown to produce reformates containing 75-80% hydrogen, whereas partial oxidation produces concentrations ranging from 65% for undiluted oxygen flows and dropping to below 50% for reactions involving air as the oxidizer (Ahmed and Krumpelt 2001; Heinzel 2002).

To address the tradeoffs between the two processes, researchers sought a compromise and developed a hybrid system referred to as autothermal reforming (ATR) which combines oxidation and reforming reactions into an overall reaction shown in Equation 1.5 (Freni et al. 2000; Ahmed and Krumpelt 2001; Heinzel 2002).

$$CH_4 + 0.5O_2 + H_2O \Leftrightarrow CO_2 + 3H_2\,,\ \Delta_R H^{\circ}_{298K} = -18.4\ \ (kJ/mol) \qquad 1.5$$

In ATR, both primary reactions occur sequentially such that the POX reactions provide the necessary heat for the reforming reactions. The exothermic pathways produce marginal gains (< 2%) in fuel processing efficiency (defined as the ratio of lower heating value of hydrogen produced to the lower heating value of fuel consumed)

because it is assumed that all of the fuel in these pathways is eventually converted to hydrogen instead of a portion being combusted as solely a heat source for reforming (Ahmed and Krumpelt 2001). However, the concentration of hydrogen in an air-fed ATR reformate product only rises to 53.9% due to nitrogen dilution from the reaction with air (Ahmed and Krumpelt 2001). This concentration is still considerably less than the 75-80% for steam reforming. Therefore, steam reforming remains an attractive candidate and would benefit from a more efficient heat source.

This study examines a reactor configuration which takes advantage of the high H_2 content achievable in reforming by using the heat produced by catalytic combustion on the opposite side of a shared surface. The reactor concept will be tested experimentally using H_2 combustion over a supported Pd-based catalyst to fuel the CH_4 steam reforming occurring in an alternate channel over a supported Rh catalyst. The dynamic relationship between the reforming and combustion channels will be investigated numerically to show the benefits of this arrangement.

1.2 COUPLING ENDOTHERMIC AND EXOTHERMIC REACTIONS

A fuel processor can be viewed as a heat exchanger with catalytic reactions. On a fundamental level, the autothermal reformer performs naturally like a heat exchanger occurring within one channel. The partial oxidation reactions raise the operating temperature and trigger the reforming reactions once steam is present in the flow. A more common perception of a heat exchanger involves separate channels where the heat exchange occurs across a shared surface. Until the recent development of catalytic

combustion technology, heat sources for sustaining endothermic reactions were hot combustion gases generated upstream of the heat exchanger or by means of a radiant burner.

An alternative approach to these gas-solid heat exchanges is to produce the heat directly at the surface through catalytic combustion reactions as shown in Figure 1.1.

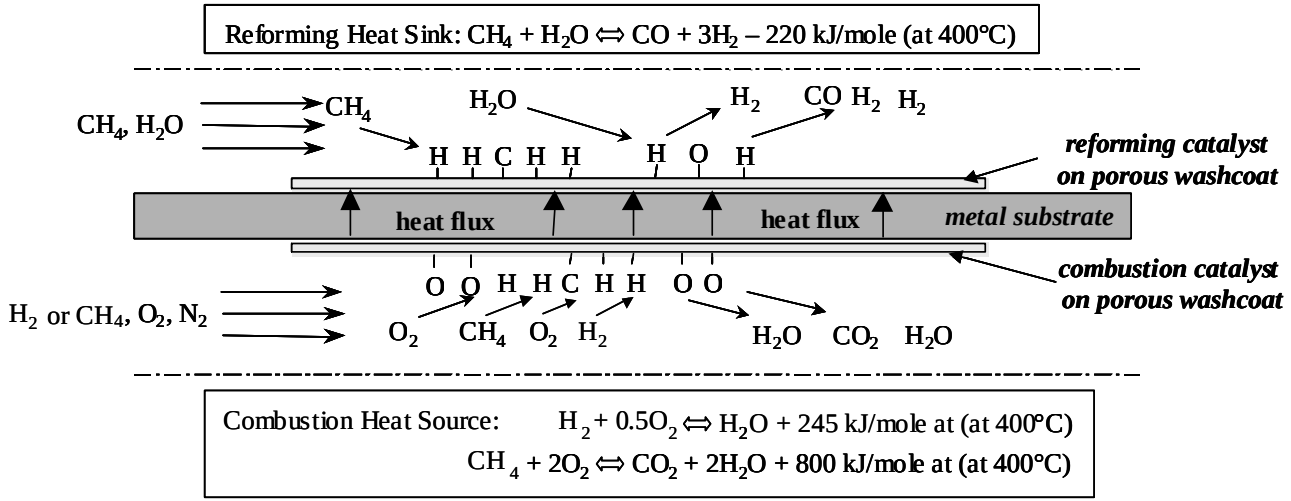

Figure 1.1 Diagram of dual channel configuration indicating combustion and reforming surface reactions and direction of heat exchange

Maximum heat fluxes for this configuration can be approximated by the product of the heat of reaction for reforming times the maximum mass transfer rate of the limiting reactant to the catalytic surface:

$$\dot{q}''_{\max} = \left(\frac{PX_{CH_4}}{RT} \right) \left(\frac{Sh_{CH_4} D_{CH_4}}{d_{chan}} \right) \Delta H_{reac} \qquad 1.6$$

In Equation 1.6, $\dot{q}''_{\max}$ represents the maximum heat flux through the surface, Sh_{CH_4} is the Sherwood number (the mass transfer analog to heat transfer's Nusselt number), D_{CH_4} is the diffusivity of methane in the reforming flow (the limiting reactant for the conditions in this study), X_{CH_4} is the inlet mole fraction of the limiting reactant, d_{chan} is the channel height, and r H_{reac} is the heat of reaction for reforming. For the conditions in the present study, T = 600°C, P = 1 atm, d_{chan} ~ 1.0 mm, V ~ 6 m/s, these surface reactions produce heat fluxes on the order of 6-8 W/cm^2, which are an order of magnitude greater than their gas-phase counterparts. These high heat fluxes provide an efficient heat source for the endothermic reforming reactions. This concept has been simulated in a co- and counterflow arrangement employing catalytic combustion and reforming of CH_4 (Frauhammer et al. 1999; Kolios 2002). Simulations indicate that with a properly designed reactor, the process is capable of achieving full methane conversion in both flows; however, temperature management for catalyst durability remains a problem, particularly in the counterflow case.

This study will seek to determine the stable operating conditions of a laboratory scale reactor employing coupled catalytic combustion and steam reforming reactions.

The experimental setup will provide valuable surface temperature measurements and real-time exhaust analysis in order to study the effect that various inlet conditions, including combustion fuel equivalence ratio (ϕ_{comb}), inlet velocity, and inlet temperature have on the transient and near steady-state performance of the reactor. The knowledge gained in the experiments will be applied to a quasi one-dimensional transient model to extrapolate into operating conditions which are difficult to study experimentally.

1.3 METHANE COMBUSTION AND REFORMING CATALYSTS

In a recent review of the complete oxidation of methane, supported palladium is reported to be the most active noble metal catalyst for low temperature lean conditions (Gelin et al. 2002). This characteristic makes palladium particularly attractive for combustion applications where low reaction temperatures are critical to achieving ultra-low emissions of NO_x and other pollutants (Forzatti et al. 1999).

The high temperature behavior of palladium has warranted considerable attention as well. Palladium based catalysts undergo a hysteretic oxidation/reduction cycle marked by a reduction of PdO $\rightarrow$ Pd between 700 and 800°C depending on the partial pressure of O_2. Reoxidation of Pd $\rightarrow$ PdO occurs at lower temperatures around 650°C (Farrauto et al. 1992; Wolf et al. 2003). This hysteresis loop can greatly affect the activity of the catalyst and the stability of any system utilizing palladium, particularly for CH_4 combustion. The phase transformation has prompted discussion regarding the most active phase of palladium for high temperature combustion applications. Some researchers argue that the oxidized state is most active (Farrauto,

Hobson et al. 1992; Burch et al. 1995) while others contest that the reduced form is preferred (Lyubovsky et al. 1999). Others have proposed alternative mechanisms for describing the active surface involving a mixed Pd/PdO state (Lyubovsky et al. 1998) or where pairs of oxygen atoms and vacancies are present (Fujimoto et al. 1998). The uncertainty of Pd oxidation states and their activity leads to complex reactor behavior that is still under investigation for catalytic combustor development (Fant et al. 2000).

Catalytic steam reforming has been extensively used for industrial hydrogen and syngas production from light hydrocarbons. Neglecting cost, rhodium catalyst presents several advantages over conventional nickel catalyst (Trimm et al. 2001). Rhodium has been shown to be a more active catalyst (Rostrup-Nielsen et al. 1977) and to be more resistant to coke formation (surface carbon build-up at high temperatures) and subsequent deactivation than nickel (Rostrup-Nielsen 1984; Trimm 1999). Despite these process advantages, there has been considerably more investigation into the kinetics of nickel-catalyzed steam reforming due to the significant cost savings in using Ni-based catalysts. Xu and Froment have proposed a 3 step reaction mechanism (Xu et al. 1989) accounting for methanation (Eq. 1.1 and 1.2) and the water-gas shift reaction shown below.

$$CO + H_2O \Leftrightarrow CO_2 + H_2, \qquad \Delta_R H^{\circ}_{298K}\,(kJ/mol) = -41.2 \;\; (kJ/mol) \qquad 1.7$$

Hou and Hughes investigated six mechanisms for Ni-based steam reforming focusing on variations in the adsorption behaviors of methane and steam (Hou et al. 2001). They found that the rate of methane conversion is proportional to the partial pressure of

methane indicating that the adsorption of methane is a rate limiting step in the reaction. They also showed that high steam content and low temperatures are keys to hydrogen production, both of which follow the water gas shift reaction in Equation 1.7.

For rhodium-catalyzed steam reforming, parallels must be drawn from partial oxidation studies because steam reforming kinetics are not yet well understood. Hickman and Schmidt studied methane oxidation over rhodium-coated monoliths at high temperatures and developed an elementary step chemistry (Hickman et al. 1993). Deutschmann improved upon this work and developed a 38-step mechanism which captures the adsorption and desorption of the major species as well as the cracking of the C-H bonds on the surface (Deutschmann et al. 1998; Schwiedernoch et al. 2003). This mechanism includes alternative hydrogen production pathways including steam and CO_2 reforming.

1.4 REFORMERS AND COMBINED GT-SOFC SYSTEMS

Hydrocarbon fuel pre-processing (either by steam reforming or partial oxidation) represents an attractive interim solution to produce H_2 for fuel cells and thereby assisting the transition to a hydrogen economy. Reformers capable of converting common fuels such as gasoline, methanol, and natural gas into hydrogen, are coupled with Polymer Electrolyte Membrane Fuel Cells (PEMFC) for propulsion power for passenger cars and Solid Oxide Fuel Cells (SOFC) for auxiliary power in heavy duty vehicles or stationary powerplants (Krumpelt et al. 2002). The reformers in PEM systems combust part of the cargo fuel or recycled anode off-gas as the heat source for

the reactions, while the reformers closely coupled to the SOFC systems can use the high operating temperatures of the fuel cell to promote the reforming reactions. As an example, a prototyped 3-kW methanol reformer was tested which used unutilized H_2 and residual impurities as the combustion fuel (Han et al. 2000). A possible reformer design combining this concept with the alternate channel configuration proposed in the current research is shown in Figure 1.2. Steam and methane enter one set of channels and are converted to H_2, CO, CO_2, and H_2O. Depending on the application, the reformate must be further purified to raise the concentration of H_2 and remove CO, especially in the case of a PEMFC where CO is damaging to the membrane. A portion of the H_2 is unconsumed in the fuel cell anode and can be reintroduced to the combustion channels before being exhausted from the system.

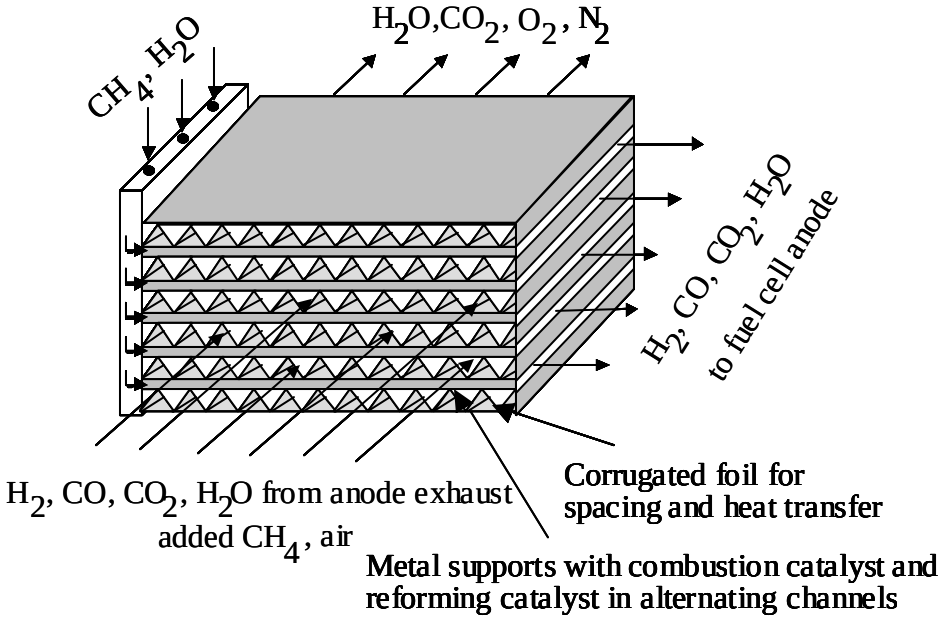

Figure 1.2 Schematic of a cross-flow, alternating channel fuel reformer showing inlet and outlet species of catalytic combustion and reforming pathways

It is most likely that CH_4 reformers will play a more significant role in stationary power plants where the increased efficiency and higher operating temperatures of solid oxide fuel cells are better suited. In an effort to recover the thermal energy produced by fuel cells, researchers developed combined cycles integrating a high temperature SOFC with a gas turbine (GT). The high electrical efficiency of the SOFC (~ 60%) combined with the expansion work produced by the gas turbine has been shown to raise fuel utilization efficiencies above 65% (Harvey et al. 1994; Palsson et al. 2000). Because SOFC's are capable of internally reforming fuels, the degree of external reforming is of particular interest to these studies. Harvey and Richter found that a pre-reformer was necessary to avoid sharp temperature gradients at the entrance of the fuel cell arising from high levels of endothermicity otherwise (Harvey and Richter 1994). They further concluded that the purely internal reforming SOFC system offered no noticeable improvement in cycle efficiency. Palsson fixed the external reforming to 30% and adjusted other parameters, such as the amount anode exhaust recirculation, to meet the pre-reformer's heat requirements (Palsson, Selimovic et al. 2000). A possible configuration of an SOFC-GT combined cycle employing the reformer design proposed in the current research is shown in Figure 1.3.

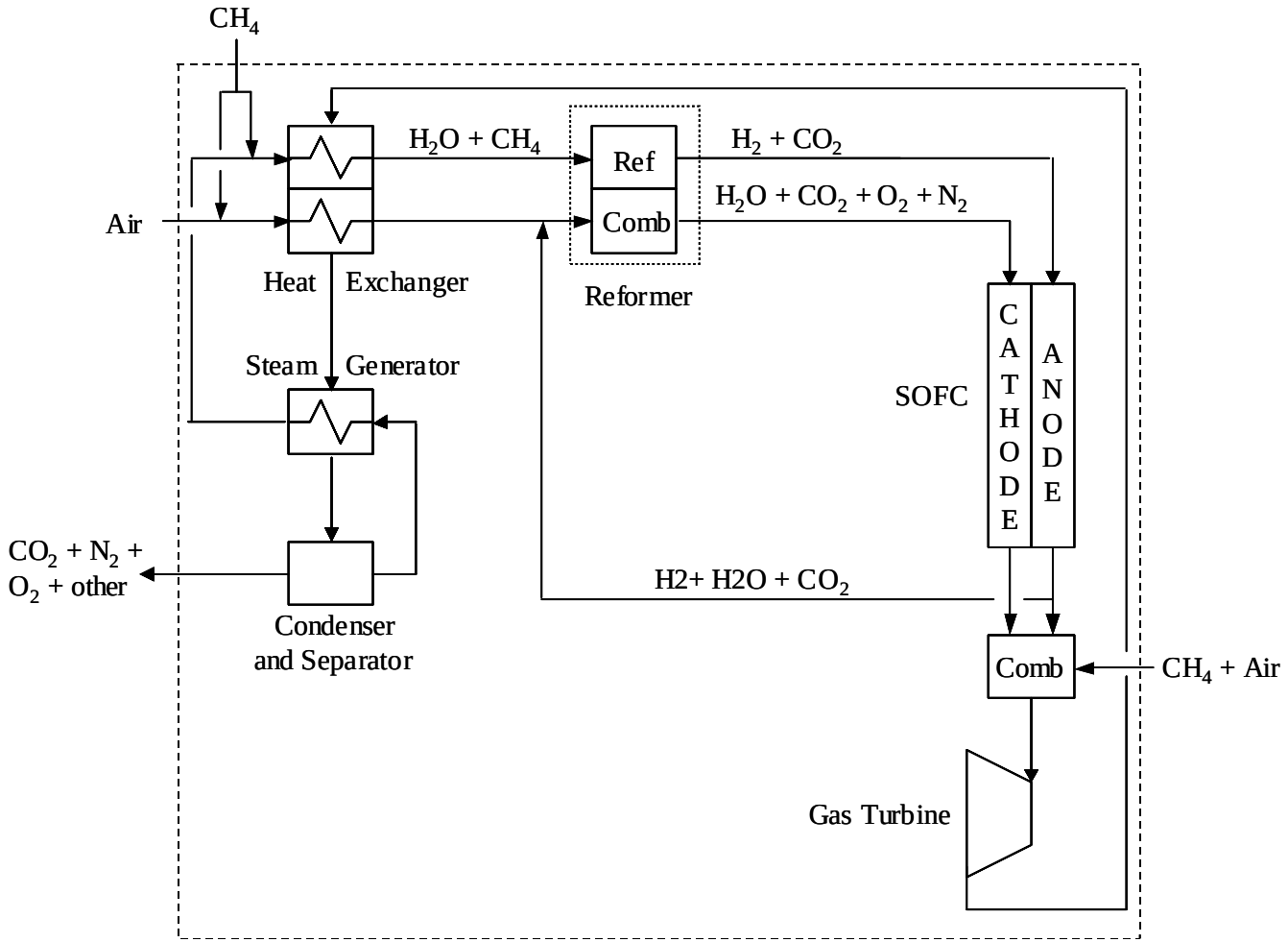

Figure 1.3 Schematic of an SOFC-GT combined cycle including the external reformer proposed in this study

1.5 OBJECTIVES OF RESEARCH

The current research proposes to study the dynamic relationship between combined catalytic combustion of H_2 or CH_4 and catalytic steam reforming of CH_4 during transient conditions when both catalysts can experience changes in activity. These changes in activity can lead to a drop in reactor performance if the high temperature reduction of the PdO combustion catalyst and low temperature coke formation on the Rh catalyst are not properly managed. Therefore, this work will focus on the thermal management of the system in order to maintain a high activity for both catalysts through the pursuit of the following objectives:

- design a laboratory scale reactor which integrates exothermic catalytic combustion and endothermic catalytic steam reforming occurring across a shared surface in alternate channels
- determine a range of stable operating conditions on a laboratory scale which is suitable for sustained CH_4 reforming and H_2 combustion
- study experimentally and numerically how the heat fluxes across this shared surface can sustain steam reforming below commonly accepted temperatures
- apply these findings to validate a transient dual channel model of the system
- explore operating conditions and reactor geometries suited for effective hydrogen production in practical applications

The thesis is arranged to present experimental and modeling work that will build upon the previous chapters. Chapter 1 has discussed the background work and the novelty of the

current research and identified the challenges it will address. Chapter 2 describes the development of the experiments designed to study a laboratory scale dual channel reactor combining catalytic combustion and steam reforming reactions. Chapter 3 presents the significant findings of the experiments and its limitations. The analysis will include surface temperature profiles and the impact that various operating conditions have on the key performance metrics: reforming fuel conversion (χ_{CH_4}) and hydrogen selectivity (η_{H_2}). Chapter 4 describes a quasi one-dimensional model adapted to handle the two different catalytic reaction channels for this study. Chapter 5 begins with a brief validation of the model with the limited experimental results and then presents a qualitative analysis on how operating conditions can impact reactor performance. Chapter 6 places the current research in perspective and conclude with a recommendation for future work.

Chapter 2

Experimental Description

2.1 INTRODUCTION

Experiments have been conducted to study the dynamic relationship between catalytic combustion and steam reforming occurring across a shared surface. To this end, a dual channel co-flow catalytic reactor has been designed to study the interactions between combustion and endothermic steam reforming. The experiments use a quadrupole mass spectrometer to measure the product concentrations in the exhaust of the reforming channel to assess the impact of combustion to reforming fuel ratio and reforming steam content on reactor performance. The purpose of these experiments is to validate a transient channel model, which will then serve as a basis for future design explorations. The experiments described in this chapter will demonstrate the complexity of the process and develop a better understanding of the transient phenomena occurring along the catalytic surfaces.

2.2 REACTOR DESIGN

The underlying goal in designing the reactor is to create a manageable self-contained unit that allows for a measure of catalyst activity and stability over a range of different conditions in both flows. The initial reactor concept addresses this issue through the incorporation of unique design features:

- two channels operating independently of one another except for the heat exchange across a shared surface
- high temperature materials for operation up to 900ºC and high levels of humidity
- accessibility for interchanging catalysts after experimental testing
- temperature measurements on catalytic surface and in bulk flow
- adequate premixing to guarantee an even distribution of species and temperature that is consistent with the model assumptions
- independent exhaust gas sampling and subsequent analysis

Because accessibility is a critical element, the reactor is designed to be modular and therefore exists as several parts which are assembled prior to testing. The components include the catalytic reactor zone, the mixing zone, the inlet and outlet manifolding, the channel gasketing, and the catalytically coated separating plate. The layout of the components, with the exception of the separating plate, is shown in Figure 2.1. Each of these components will be described in further detail.

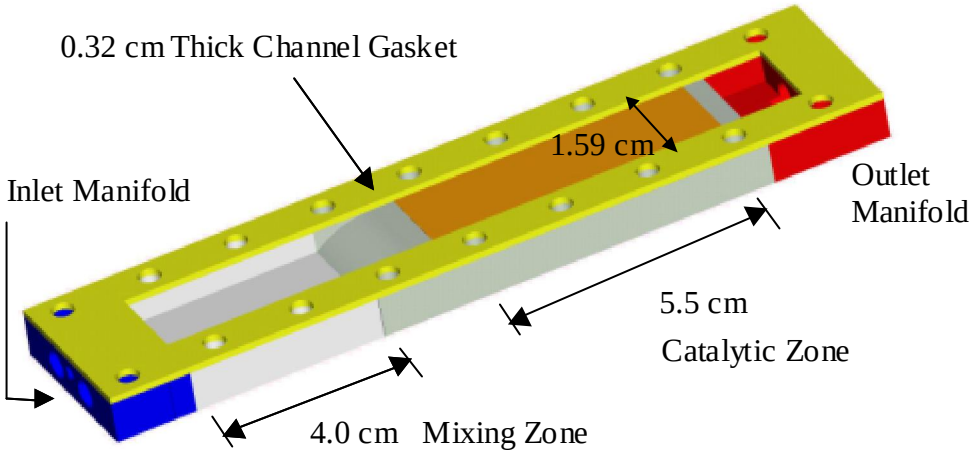

Figure 2.1 Layout of one half of the catalytic reactor housing showing the inlet manifold, mixing zone, location of the catalytic zone, outlet manifold and channel gasket. Not shown is the separating Fecralloy substrate where the catalysts are applied on opposed sides

Introducing the flows into the combustion-side of the reactor presents a design challenge because of the need to preheat the streams while preventing undesirable premature gas-phase reactions. Therefore, a manifold has been constructed to inject the fuel into the oxidizer downstream of the preheaters and closer to the catalyst. The inlet manifold is composed of two parts. The first section splits the single air flow leaving the heater into two streams. The second section (Figure 2.2) is comprised of two plates sandwiched together with three inlet holes and two outlet holes. The downstream plate has grooves extending from a shallow center well forming channels connecting the center inlet hole to the outer flow paths. The fuel is injected into the center port and forced outwards through the channel grooves into the oxidizing streams which are expanded into the reactor. Although the reforming-side inlet has a similar manifold, the reforming fuel is actually injected upstream of the preheater since pre-reactor reforming reactions are not a risk.

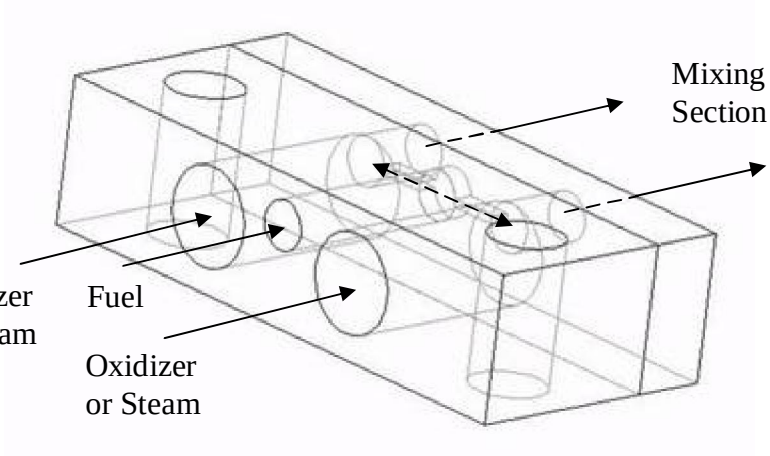

Figure 2.2 Hidden view drawing of inlet manifold showing how the fuel and oxidizer are mixed on the combustion side

Downstream of the inlet manifold the injected flows enter a 4 cm long mixing zone that is loosely packed with quartz wool. Potential dead zones near the entrance have been filled with ceramic board to reduce the likelihood of autoignition. The mixing zone concludes with a coarse Hastelloy X honeycomb to even out any remaining inconsistencies. The flows next proceed up a ramp and encounter the catalysts. The reaction zone has a cross-section of 0.32 cm high x 1.59 cm wide and extends 5.5 cm through the reactor.

Temperature measurements in these sections of the reactor and a desire to maintain a robust design dictate the construction material possibilities. Although dual channel experiments can be performed without prejudice to material selection, single channel experiments, conducted between separate catalytically coated substrates, require the thermocouples to contact the reactor walls. Dual channel experiments avoid this predicament since the thermocouples and substrate reside between layers of gasketing. Thus to accommodate both geometries, the reactor walls were initially made from ceramic which is electronically isolating. Difficulties in sealing the reactor housing

resulting from the mating of materials with significantly different thermal expansion properties became prohibitive. The final design replaces the ceramic housing of the mixing and reaction zones with sections machined from stainless steel. These sections are welded to the existing Hastelloy X (mostly Fe/Cr/Mo) inlet and outlet manifolds with the advantage of better sealing but at the expense of a less robust design.

The gaskets provide sealing along the length of the reactor. Since the reactor has been machined from different materials and welded together, surface imperfections, particularly weld beads, require the gasket to be pliable to ensure proper sealing. In addition to sealing, the gasket forms the channel sidewalls via a slot cut through its center as shown in Figure 2.1. The channel formed is bordered on the sides by the gasket and above and below by the non-catalytic reactor wall and catalytic separating plate. Utilizing the gasket in this fashion permits quick modification to the channel dimensions. For example, a larger channel height can be accomplished by simply using a thicker gasket. For the purpose of this study, the channel dimensions remain fixed (1.59 cm wide x 0.32 cm tall x 5.5 cm long in the reaction zone). Finally, the gaskets also make the reactor accessible for thermocouple wires such that the wires are fed between two electrically isolated surfaces.

The separating plate resides between the gaskets and splits the reactor into two identical channels. The substrate is a 1 mm thick plate of Fecralloy (Fe 72.8/ Cr 22/ Al 5/ Y 0.1/ Zr 0.1), which has a thermal conductivity of 16 W/m/K. Fecralloy was selected because it provides a durable high temperature metal substrate which is commonly used in catalytic combustor monoliths. When sintered at high temperature, a passivating

Al_2O_3 layer is formed on the surface to protect the metal. The portion of the plate in the reaction zone is coated on both sides with either the reforming or combustion catalyst.

2.3 FLOW PREPARATION

Steam is introduced into the reforming flow using a bubble saturator made of Pyrex glass. Diluent is passed through a stainless steel tube entering through the top of the saturator and exiting through a coil at the bottom. The coil is dotted with holes spaced sufficiently apart to prevent the rising bubbles from coalescing. The column of water is maintained at a suitable height to ensure that the bubbles reach saturation before leaving through an orifice centrally located at the top of the saturator. The saturation temperature is defined as the temperature of the humidified diluent exiting the saturator and is measured by a shielded K-type (alumel/chromel) thermocouple. The saturation temperature is controlled by adjusting a hot plate below the saturator assembly. The entire saturator is wrapped in carbon gasketing to provide good conduction from the hotplate heater to the walls of the saturator and thus, to promote quicker thermal equilibrium throughout the column of water. The flow rates of all of the gases in the experiment are controlled by Brooks 5850E mass flow controllers.

The single plate reactor investigated in this study represents only a subset of a multi-channel monolithic design and as such, measures have been taken to create a suitable thermal environment to simulate the multi-channel version. Even with this enhanced heat transfer configuration, noticeable steam reforming begins when the surface reaches 600ºC. Therefore, preheating of the flows is necessary to achieve these

temperatures across the majority of the catalytic zone while operating the combustion side under lean conditions. The flows are preheated between 350ºC and 450ºC using electric heaters. In addition to preheating, the reactor is housed in a Lindberg/Blue M temperature programmable tube furnace to simulate an adiabatic environment by reducing the heat loss through the reactor walls. The furnace is maintained at the reactor inlet temperature which is typically 400 – 500ºC. Since these inlet temperatures fall below the stable operating range for the reforming reactions (600 – 900ºC), reforming fuel is not introduced into the reactor until the catalytic combustion has raised the surface temperatures sufficiently. A layout of the experiment showing the location and plumbing of the flow preparation components is shown in Figure 2.3.

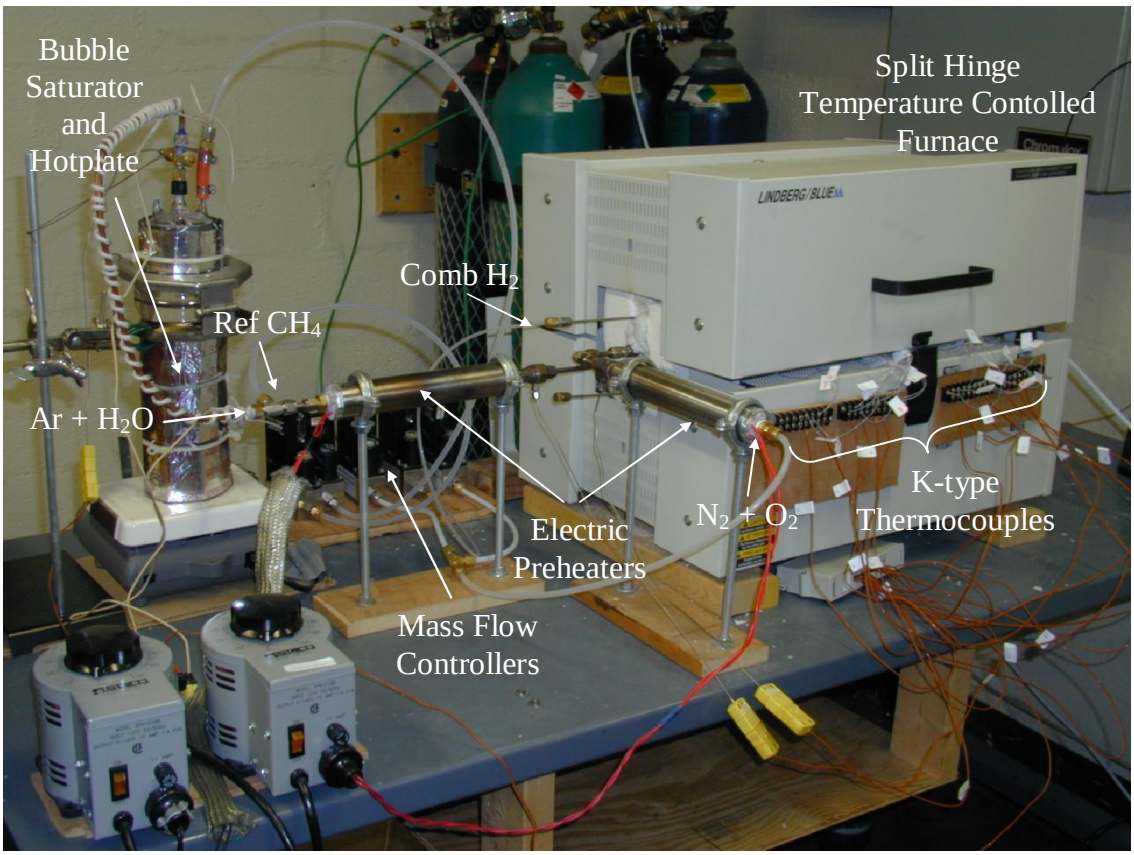

Figure 2.3 Layout of dual channel experiment including flow preparation components and temperature controlled furnace housing the reactor

2.4 DIAGNOSTICS

Temperature measurements are essential to understanding the dynamics of the catalytic reactions; however, they are difficult to measure accurately for high temperature surface reactors. Surface temperature measurements indicate the progress of the reactions and their preferred location within the catalytic region. Channel flow measurements are used to monitor inlet and exhaust temperatures and provide alerts in the case of flashback or premature gas-phase combustion upstream of the catalyst. With the exception of the saturator and preheaters, all temperature measurements are made from 0.005" diameter bare wire K-type thermocouples. The thermocouple leads are electrically isolated from one another as they exit the furnace using a combination of ceramic and plastic tubing as shown in Figure 2.4. The signal from each of these thermocouples is read by a data acquisition system and monitored using Labview. A Labview program was developed for the experiments to control the mass flow controllers, record the temperature measurements, and present real-time updates of the experiment. The temperature measurements are coordinated with exhaust gas analysis post-experiment to provide a total picture of the activity of the catalyst and the progression of the reactions with respect to time.

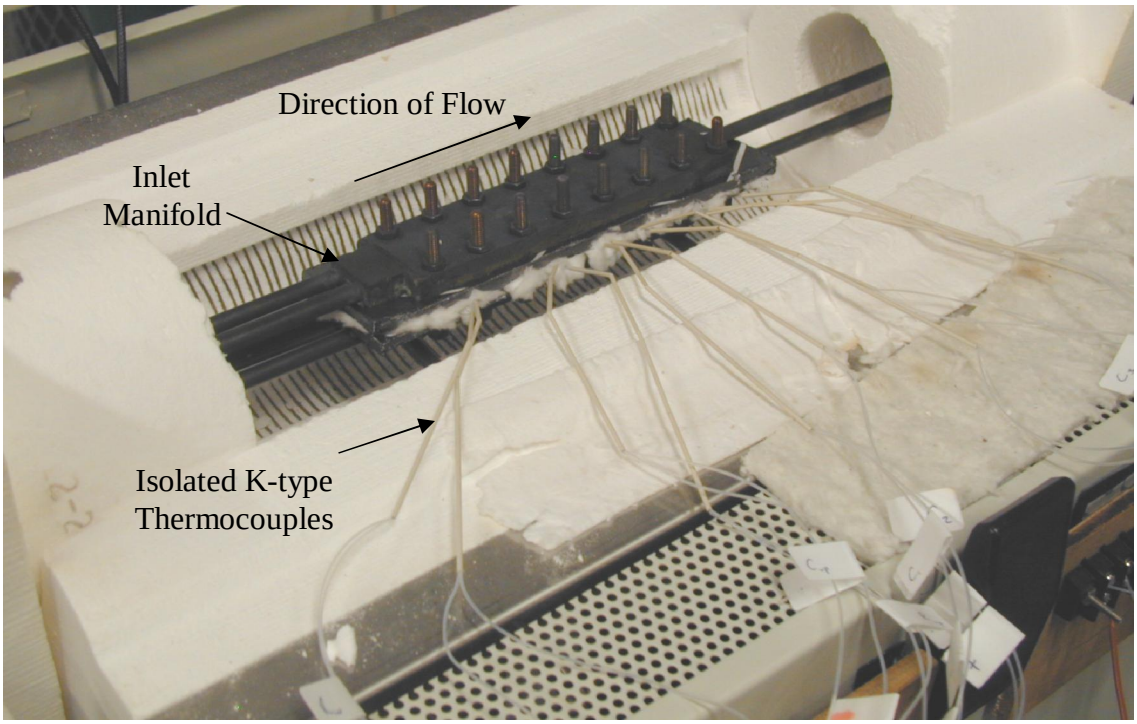

Figure 2.4 K-type thermocouples extending from reactor interior to terminal blocks outside of furnace showing the measures taken to keep them isolated

Surface temperature measurements are made by tack welding the thermocouple beads directly to the separating plate along the 5.5 cm reaction zone as well as upstream of the catalyst. After several iterations, it was determined that the best time to attach the thermocouples was following the application of the catalyst. Therefore, a small portion of the catalyst, roughly the size of the thermocouple bead (~1 mm^2), was removed just prior to tacking the thermocouples. The layout of the surface thermocouples on the plate is shown in Figure 2.5. Surface temperature measurements made upstream of the reaction zone (labeled C_{up} and R_{up}) provide insight into upstream heat conduction along the separating plate.

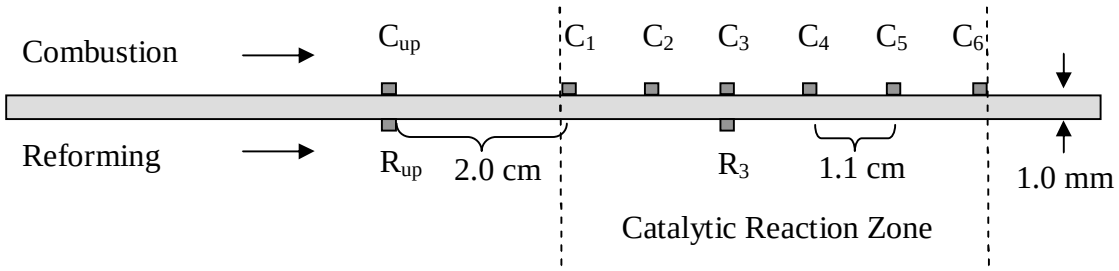

Figure 2.5 Layout of thermocouple placement on Fecralloy substrate

In order to capture transients during the reaction start-up and changes in catalyst activity, a mass spectrometer is used for exhaust gas analysis. A mass spectrometer measures the concentration of species present in a stream based on their mass-to-charge ratio. These experiments use a Quadrupole Mass Spectrometer (QMS), Gaslab 300 model from VG Gas Analysis Systems. The QMS operates by ionizing the incoming stream and allowing the positively charged ions to pass through to the mass filter. Inside the filtering chamber, two pairs of rods apply constant (dc) and alternating (ac) electric fields which allow only a select ion to reach the detector. By varying the fields, a range of mass-to-charge ratios is detected. On-board analysis capabilities allow concentrations to be updated every 8-10 seconds. From these concentrations, reforming fuel conversion (Eq. 2.1) and hydrogen selectivity (Eq 2.2) can be calculated.

$$\chi_{CH_4} = 1 - \frac{n_{CH_4,out}}{n_{CH_4,in}} \qquad 2.1$$

$$\eta_{H_2} = \frac{n_{H_2,out}}{n_{H_2,\max\ achievable}} \qquad 2.2$$

Reforming fuel conversion describes the fuel consumption and varies between zero and one. Selectivity refers to the process's ability to generate the desired product, hydrogen. Recalling the two major pathways for the complete steam reforming methane reactions, Eq. 1.1 and 1.2, a maximum of four moles of hydrogen and a minimum of three moles of hydrogen can be formed when one mole of methane reacts with steam. Thus hydrogen selectivity varies between 0.75 and 1.00. This selectivity range holds even in a wet (Eq. 2.3) or dry (Eq. 2.4) environment as the overabundant reactant is passed on.

$$CH_4 + 3H_2O \Leftrightarrow CO_2 + 4H_2 + H_2O \qquad 2.3$$

$$2CH_4 + H_2O \Leftrightarrow CO + 3H_2 + CH_4 \qquad 2.4$$

The mass spectrometer requires frequent calibration when not operated continuously to ensure accurate measurements and reduce background effects. The QMS should be calibrated every few days of operation for all relevant gases. For the reforming

experiments in this study, calibration is performed on methane (CH_4), hydrogen (H_2), carbon monoxide (CO), carbon dioxide (CO_2), and argon (Ar). Water is excluded from this list since the QMS has difficulty handling moisture due to water adsorption along the capillary sampling line and inside the mass spectrometer vacuum chamber. The effects of water must be post-processed out. Calibration should be performed on controlled mixtures of gases which are representative of the experiments.

A drawback when using mass spectrometry is that it depends almost entirely on molecular mass. This dependency becomes a concern when two species of similar mass are to be analyzed and differentiated. In the case of reforming experiments, this situation arises since carbon monoxide is a major product and has the same weight of 28 gmol/mol as nitrogen (N_2). Therefore, argon with a weight of 40 gmol/mol has been chosen as the reforming diluent. Additionally, the abundance of nitrogen in the air surrounding the experiment requires the reactor and sampling lines to have minimal leaks; otherwise, any air leaks will produce a false CO mole fraction in the measurements. Background CO measurements were taken prior to each reforming run to approximate the level of air leakage into the reactor. These backgrounds were removed during post-processing as will be further explained in Chapter 3.

2.5 CATALYSTS AND SUPPORT MATERIALS

The catalysts are selected based upon their potential use in real-life applications, the availability of validated surface chemistry mechanisms which capture their kinetics, and their proven laboratory activity. Chapter 1 addresses the first two criteria and

certifies the use of palladium as the combustion catalyst and either nickel or rhodium as the reforming catalyst. Previous laboratory results at UMCP (Zhu 2001) demonstrate the activity of supported palladium catalyst for lean methane combustion; however, additional reforming catalyst testing has been carried out for this study.

Catalyst characterization tests have been performed separately on supported nickel and rhodium catalysts to determine which is most active and stable for the testing conditions in the dual channel study. The testing configuration is modeled after other researchers (McCarty et al. 1994; G. Groppi 2001). A non-porous α-Al_2O_3 tube (9.5 mm diameter) is coated with a thin porous γ-Al_2O_3 or $MgAl_2O_4$ washcoat (30-40 μm thick) which has been impregnated with either nickel or rhodium catalyst. The catalytically active region (20 mm long) is centrally located inside a quartz tube creating a narrow annulus for the passing flow (approximately 0.5mm high including washcoat). The entire reactor is maintained inside a split tube furnace to ensure isothermal conditions which have been set to the inlet temperature. Backside temperature measurements are made with K-type thermocouples positioned inside the non-porous substrate at the front and back ends of the catalyst. Exhausts gas analysis is performed using the QMS in the same manner as the primary experiments of this study.

Temperature ramp tests are one of the easiest and most common techniques for determining catalytic activity over a defined temperature range. For these tests, a series of temperature ramps between 700 – 900ºC at 5ºC/min is imposed on the catalyst while holding the inlet steam to carbon (H_2O:CH_4) ratio at 1.25 and velocity at 9 m/s. A sample of the results for the rhodium catalyst is shown in Figure 2.6 which demonstrates its sustained high activity over the entire ramp. The results from the nickel tests (not

shown here) show reduced conversion without the stability of Rhodium for the same temperature range. Therefore rhodium has been selected for the dual channel experiments. This is in agreement with the reported literature (Rostrup-Nielsen 1984).

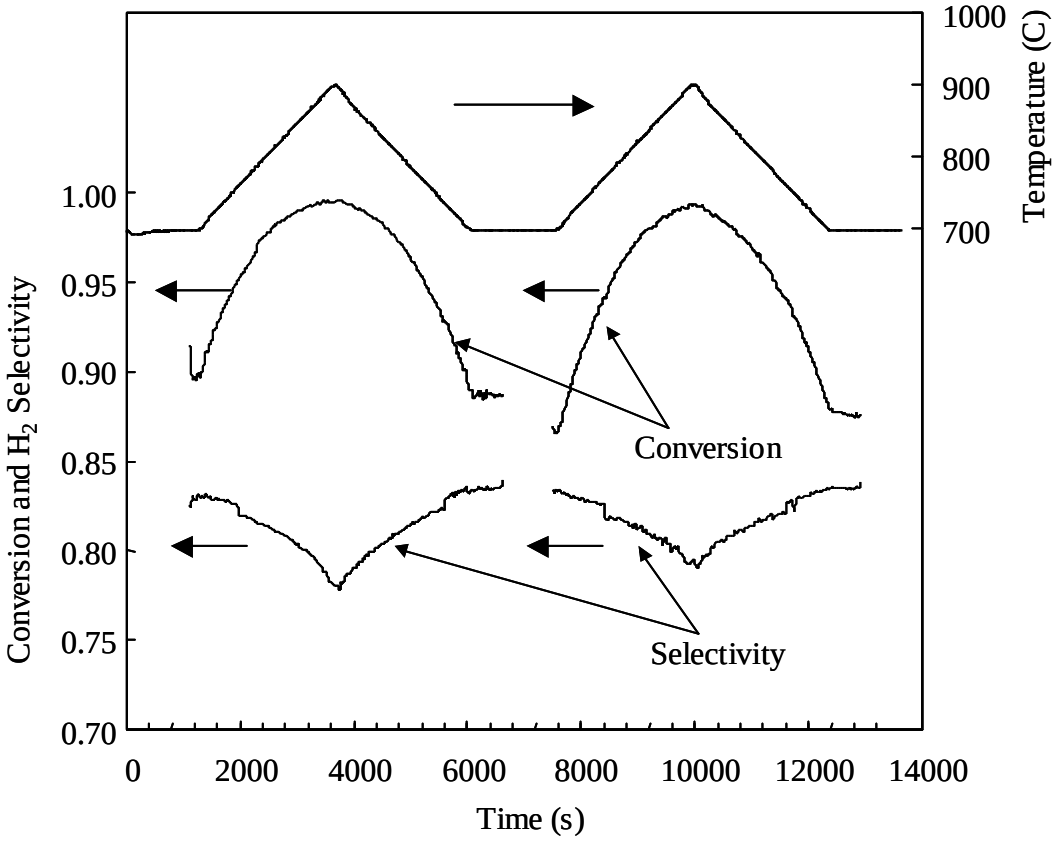

Figure 2.6 Transient CH_4 conversion and H_2 selectivity for consecutive temperature ramps from 700-900°C imposed over alumina supported Rh catalyst.

For the ultimate dual channel experiments, the Fecralloy substrate is prepared. Prior to coating, the substrate is oxidized in a muffle furnace for 12 hours at 1100ºC. Next, a γ-Al_2O_3 washcoat is applied to both sides and baked at 150ºC for 30 minutes and then raised to 600ºC for 12 hours. The ensuing washcoat is 20 – 40 μm thick. Next, one side of the plate is coated twice by incipient wetness with a $PdNO_3$ solution which is 1% Pd by weight and then calcined at 150ºC for 30 minutes and at 650ºC for 8 hours.

Finally, the other side is coated twice with a 1% Rh by weight $RhNO_3$ solution and calcined similarly to the $PdNO_3$.

2.6 TESTING CONDITIONS

Stable operation of the alternating channel monolithic reactor concept resides within a narrow window due to the somewhat conflicting preferred conditions for each catalyst. The rhodium catalyst promotes effective reforming above 600°C, and the higher temperatures prevent coke formation or surface carbon build-up (Rostrup-Nielsen and Trimm 1977; Trimm 1999). On the other hand, the palladium catalyst can lose activity above 900°C due to reduction of the active oxide layer (Wolf, Zhu et al. 2003). In the laboratory setting when only one set of channels is studied, this conflict is exacerbated by the reliance upon one channel to supply all of the necessary heat and the extensive heat loss in the opposite direction out of the reactor. In a multi-channel configuration, the heat distribution would be more uniform with all adjacent channels contributing mutually to the heat exchange. Ideally, the process is intended to be run autothermally where all of the heat produced through the combustion is consumed by the reforming. Experiments were initially geared towards autothermal methane combustion and reforming, but combustion-only tests quickly showed the inability of methane to generate suitable surface temperatures. As a practical alternative, hydrogen is substituted as the combustion fuel. Hydrogen, which combusts over palladium more readily than methane down to temperatures as low as 100°C (Kramer et al. 2003), is present as unconverted fuel in fuel cell anode exhaust. Despite this substitution, the experiments still require

additional combustion to account for heat loss out of the reactor and the thermal mass of the separating plate, thus prohibiting autothermal operation.

Experimental conditions have therefore been established to produce sufficiently high surface temperatures and measurable changes in reactor performance. In order to generate surface temperatures above 600ºC throughout the entire catalytic zone, the combustion channel is operated at equivalence ratios (ϕ) ranging 0.3 – 0.4 and at a constant inlet velocity of 6 m/s. The reforming channel inlet velocity is varied between 1 – 3 m/s and the CH_4:H_2O ratio between 0.5 – 1.1 to observe the effects that steam content and $H_{2,comb}$:$CH_{4,ref}$ fuel ratio have on conversion and selectivity.

Chapter 3

Experimental Results

3.1 INTRODUCTION

Chapter 3 presents and discusses the results gathered from the experiments described in Chapter 2. This chapter begins with an explanation of the data reduction process to illustrate how the operating parameters (namely steam to carbon ratio, reforming fuel conversion, and hydrogen selectivity) are determined from experimental measurements. Although the experiments were intended to be conducted adiabatically, the results show the contrary and discuss the impact the heat loss had on the reactor performance.

3.2 DATA REDUCTION

As discussed in Chapter 2, the steam content in the reforming flow is controlled by the temperature inside the bubble saturator. The diluent flow exiting the saturator is assumed to be fully saturated and therefore contains a moisture content relative to the saturation pressure of steam. The steam to carbon ratio entering the reactor is determined by the ratio of the molar flow rates:

$$S/C = \frac{\hat{n}_{H_2O}}{\hat{n}_{CH_4}} \qquad 3.1$$

where

$$\dot{n}_{H_2O} = \frac{P_{H_2O}}{1 - P_{H_2O}} \dot{n}_{dil} \quad \text{and} \quad P_{H_2O} = \frac{P_{sat}(T_{saturator})}{P_{tot}}$$

The mass spectrometer, which operates as a vacuum system, is very sensitive to the presence of water (above 1% H_2O). Measuring the products from the incomplete steam reforming reaction therefore poses a problem as residual moisture will always be present. To address this concern, the mole fraction of each species measured by the mass spectrometer ($X_{k,raw}$) is normalized by removing the effects of the water:

$$X_{k,dry} = \frac{X_{k,raw}}{1 - X_{H_2O}} \tag{3.2}$$

In addition, testing was structured to take advantage of periods of stable combustion operation. Several runs of various reforming characteristics could be evaluated by allowing brief intervals, on the order of minutes, between each set of testing conditions. The background effects of any residual products desorbing from the catalyst during periods of inactivity are then averaged and removed. The resulting values represent the dry molar concentrations of each product species:

$$X_k = X_{k,dry} - X_{k,background} \tag{3.3}$$

where

$$X_{k,background} = \overline{X}_{k,dry,nofuel}$$

From these processed molar concentrations, the two principal parameters of interest, reforming fuel conversion (χ_{CH_4}) and hydrogen selectivity (η_{H_2}), are determined. The reforming reaction generates additional moles of molecules; however, atomic moles are still conserved. Conversion is calculated by measuring the

transformation of elemental carbon from methane (CH_4) to carbon monoxide (CO) and carbon dioxide (CO_2). The conversion (χ_{CH_4}) is calculated as the ratio of the converted carbon out to the total carbon fed to the reactor:

$$\chi_{CH_4} = \frac{X_{CO} + X_{CO_2}}{X_{CO} + X_{CO_2} + X_{CH_4}} \tag{3.4}$$

Hydrogen selectivity (Equation 3.5) is most easily measured by observing the ratio of CO_2 to CO. If the carbon species are primarily converted to CO_2 then Equation 1.1 is the dominant pathway and η_{H_2} approaches a maximum value of unity. On the other hand, if CO is a principal product, then the reaction proceeds according to Equation 1.2 and η_{H_2} approaches a minimum value of 0.75.

$$\eta_{H_2} = \frac{4 \cdot \frac{X_{CO_2}}{X_{CO}} + 3}{4 \cdot \frac{X_{CO_2}}{X_{CO}} + 4} \tag{3.5}$$

This equation assumes that the fraction of carbon converted to species other than CO or CO_2 is negligibly small, which from investigating off-peaks in the mass spectrometer analysis appeared to be an acceptable assumption. Applying the above definitions for fuel conversion and hydrogen selectivity and performing the remaining elemental balances for O and H atoms, the complete steam reforming reaction is developed:

$$\begin{aligned} & n_{CH_4,in} CH_4 + n_{H_2O,in} H_2O + n_{dil,in} Dil \rightarrow \\ & n_{CH_4,in}\left(1 - X_{CH_4}\right) CH_4 + \left(n_{H_2O,in} - n_{CH_4,in}\left(4 X_{CH_4} \eta_{H_2} - 2 X_{CH_4}\right)\right) H_2O + n_{dil,in} Dil \\ & + n_{CH_4,in}\left(4 X_{CH_4} \eta_{H_2}\right) H_2 + n_{CH_4,in} X_{CH_4}\left(4\eta_{H_2} - 3\right) CO_2 + n_{CH_4,in} X_{CH_4}\left(4 - 4\eta_{H_2}\right) CO \end{aligned} \tag{3.6}$$

3.3 RESULTS AND DISCUSSION

3.3.1 Transient Surface Temperature Measurements

One of the more challenging aspects of these experiments involved measuring temperatures within the reactor, particularly on the surface in the catalytic region as discussed in Chapter 2. In total, there are seven temperature measurements along the catalytic surface, two upstream of the reaction zone, and four gas-phase measurements. The transient temperature profiles recorded during one period of testing are shown in Figure 3.1 illustrating how the surface temperature profile has developed in a combustion-only mode of operation and how it then responds to changes in reforming conditions.

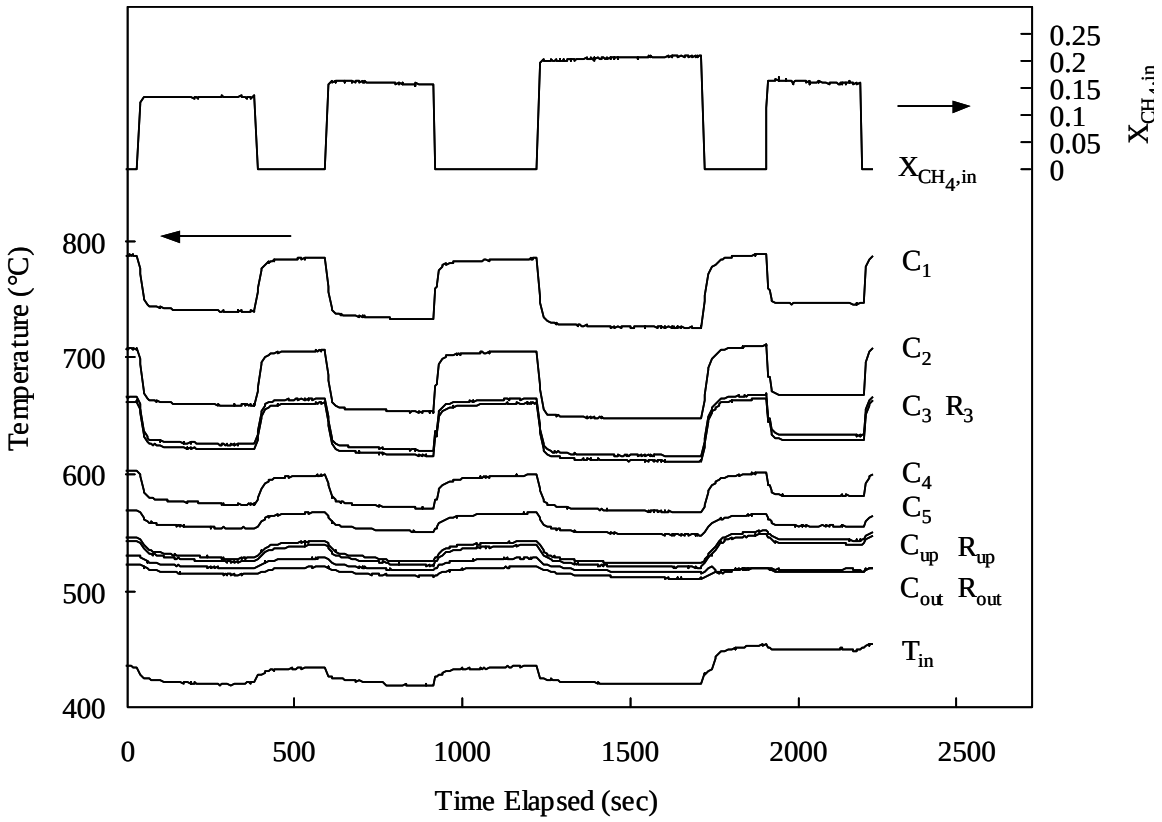

Figure 3.1 Temperature profiles of reactor temperatures under reforming conditions

The highest temperatures are found at the front end of the catalyst where nearly all of the combustion fuel is consumed. The temperatures then drop as the fuel-depleted flow progresses downstream due to the heat loss out of the reactor and the heat drawn through the Fecralloy substrate by the reforming reactions in the adjacent channel. The positions indicated in Figure 3.1 were previously identified in Figure 2.5. Surface temperatures at equivalent axial locations (C_3-R_3 and C_{up}-R_{up}) are nearly identical, indicating the high degree of conduction occurring through the catalytic surface and the near steady-state condition of the experiment. Figure 3.1 also demonstrates how the reforming inlet mole fraction affects the heat flux and how the largest delta T occurs at the front end of the catalyst.

Reacting flows operate along several different time scales. For example, adsorption and desorption of species, dissociation of species on the surface, and chemical reactions typically occur in mere fractions of a second ($\sim 10^{-8}$s) whereas diffusion into and out of the bulk catalyst can be on the order of minutes. Figure 3.1 shows the rapid response of the system marked by emphatic spikes and drops in temperature when the reforming fuel is turned on and off. The gradual rise or decay in temperature following the fast transients could be attibuted to changes in the bulk surface or the slower modes of heat transfer which now dominate the progress of the reaction.

3.3.2 Effect of X_{CH_4} on Heat Flux at Front of Catalyst

The reforming fuel inlet mole fraction was shown to have a profound effect on the front end surface temperature. Equation 1.6 from Chapter 1 describes the maximum heat flux which can be pulled through the shared catalytic surface by the reforming flow.

$$q''_{\max} = \left(\frac{PX_{CH_4}}{RT} \right) \left(\frac{Sh_{CH_4} D_{CH_4}}{d_{chan}} \right) \Delta H_{reac} \qquad 1.6$$

While the temperature may vary and the heat of reaction will change depending on the principal reforming pathway, the heat flux is primarily a function of reforming fuel mole fraction, X_{CH_4}. Under this assumption, Figure 3.2 shows how the heat flux represented by the change in front end surface temperature (or delta T) increases with fuel content. The delta T shown in Figure 3.2 is calculated as the change in the temperature measurement at the front end of the catalyst (location C_1 in Figure 2.5) between combustion-only operation and during reforming. Claiming that the change in temperature is representative of the heat flux assumes that the plate is at steady-state and the majority of the heat transfer is through the plate into the reforming channel. The inlet composition was varied by controlling not only the steam to carbon ratio, but also the amount of dilution in the reforming flow.

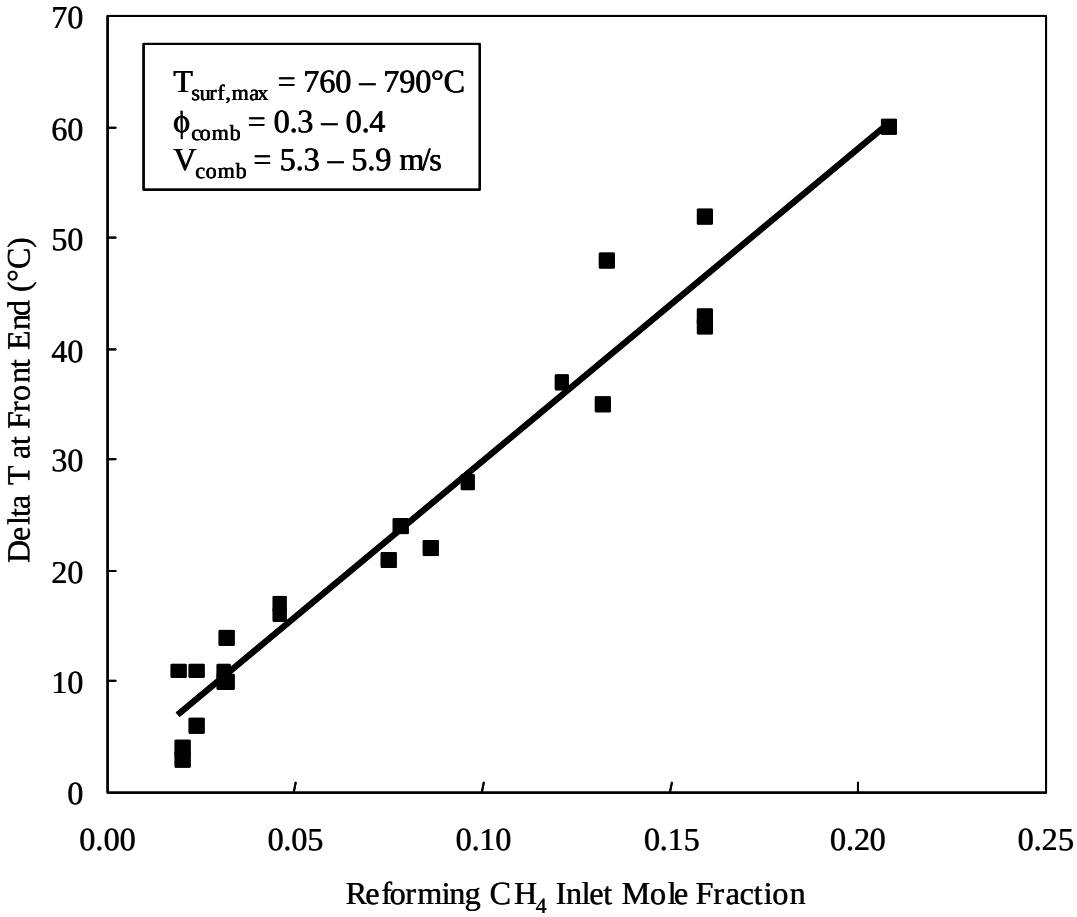

Figure 3.2 Plot of reforming fuel inlet mole fraction and its impact on front end surface temperatures

It should be noted that the surface for each point in Figure 3.2 began at relatively the same temperature and that the highest delta T was not necessarily witnessed at the highest initial temperature. In a co-flow configuration, the front end is the location of maximum heat flux where fuel content in both the reforming and combustion channels is a maximum. This configuration is therefore advantageous over a counterflow arrangement from a standpoint of temperature stability, because the pairing of the high rates of reforming and combustion promote better surface temperature mitigation.

3.3.3 Effect of the Ratio of Fuel Moles Burned to Moles Reformed on Reforming Fuel Conversion

Figure 3.3 shows steady state reforming fuel conversion plotted against the ratio of the moles of fuel fed to the combustor to the moles of fuel fed to the reformer. The moles of hydrogen burned are divided by a factor of four to illustrate the oxygen consumption relative to methane combustion. The mass transfer limited conversion is a term often associated with reacting flows and describes a process where the maximum achievable conversion is limited by the diffusion of the limiting reactant from the bulk flow to the surface.

$$\chi_{fuel} = 1 - \exp\left(-\frac{z\ k_{fuel} a_{cat}}{u}\right) \tag{3.7}$$

where a_{cat} is the ratio of the surface area of the catalyst to the volume of the washcoat; z is the length of the catalyst; u is the flow velocity; and k_{fuel} is the mass transfer coefficient:

$$k_{fuel} = \frac{Sh_{fuel} D_{fuel}}{D_h} \tag{3.8}$$

recalling that Sh_{fuel} is the Sherwood number, D_h is the hydraulic diameter and D_{fuel} is the binary diffusivity for the fuel in dilution. At these high inlet temperatures (>400ºC) the mass-transfer limited conversion in the combustion channel is near 100% within 0.1mm of the entrance to the catalyst. Therefore, it is safe to assume that nearly all of the hydrogen is consumed near the front end of the catalyst under the experimental conditions.

Figure 3.3a refers to data collected following proper calibration of the mass spectrometer and is considered quantitatively reliable. The data shown in Figure 3.3b was not collected following a complete calibration for all relevant gases and is only included to show the qualitative effect that velocity has on reforming fuel conversion. Figures 3.3a and 3.3b show the expected increase in conversion with an increase in fuel energy to the combustion channel. The additional fuel burned provides more heat to fuel the reforming reactions occurring in the adjacent channel. Figure 3.3a also shows that when the steam to carbon ratio is increased to 2.0, reforming fuel conversion drops most likely as a result of the increased competition for active adsorption sites by the additional steam. Figure 3.3 further demonstrates the inability of the furnace surrounding the reactor to maintain an adiabatic environment because of the high fuel flow rates required to achieve these levels of conversion. Modeling results in Chapter 5 will show that the ratio of combustion fuel to reforming fuel consumption should be much less than one when the reactor is operating in a near adiabatic condition.

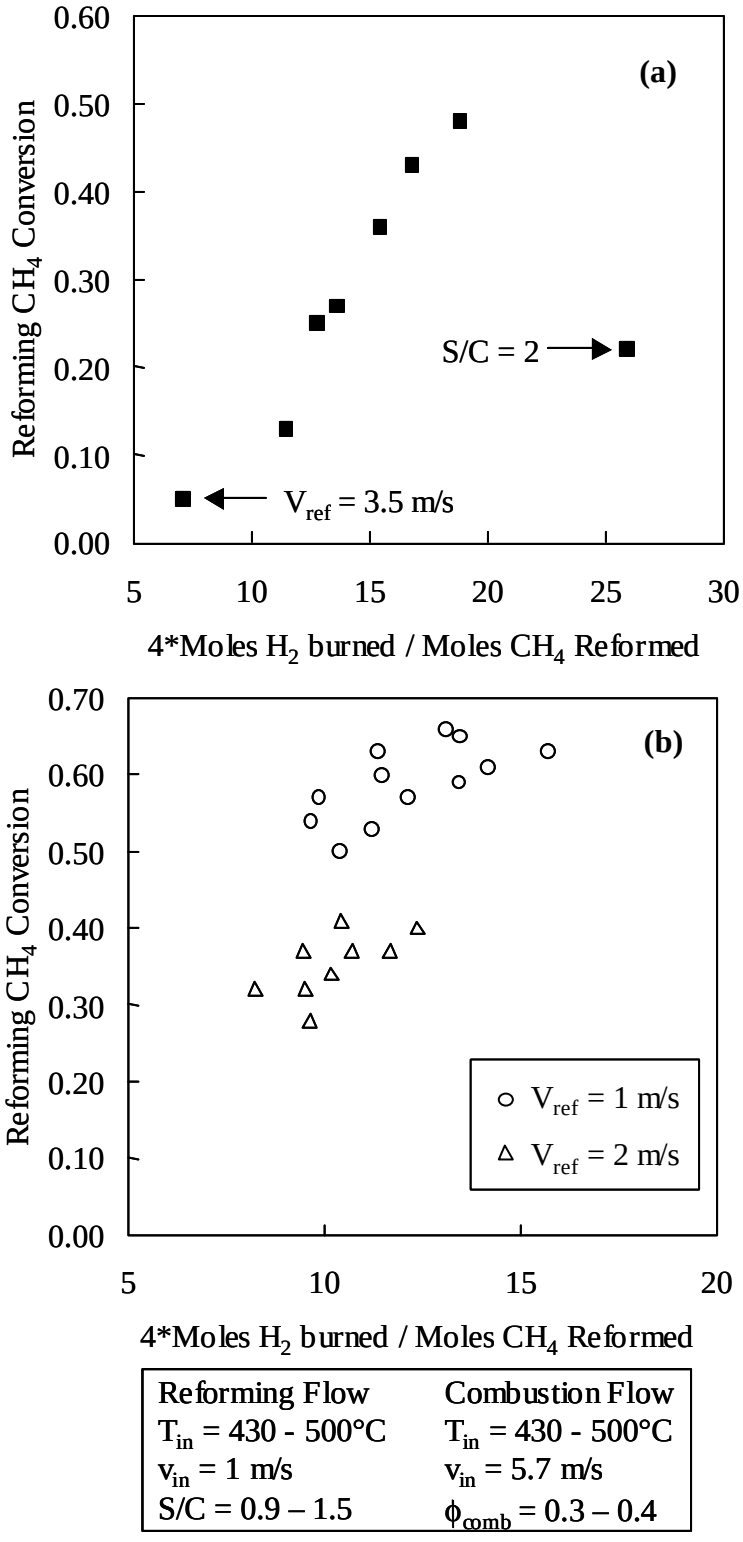

Figure 3.3 Reforming CH_4 conversion as a function of the ratio of moles of fuel to the combustor to the moles of fuel to the reformer for experimental cases (a) with proper mass spectrometer calibration and (b) without calibration

The heat loss from the reactor can be calculated by comparing the inlet and outlet enthalpies for both channels. For example, in the case shown in Figure 3.3 with X_{CH4} = 0.48, the combustor is fed 36 moles of H_2 for every mole of CH_4 fed to the reformer. The combustor is operating at ϕ_{comb} = 0.4, while the reformer is flowing 50 moles of argon and 1.5 moles of steam per mole of methane. The measured gas-phase exit temperature rises only 50°C from T_{in} = 430°C and it is assumed that all of the H_2 is converted to H_2O in the combustion channel. Table 3.1 summarizes the enthalpy change for the case shown in Figure 3.3 where χ_{CH_4} = 0.48 and includes a theoretical fuel ratio to produce the same level of reforming under autothermal, adiabatic mass-transfer-limited conditions. The comparison in Table 3.1 shows that nearly 50 times more fuel must be consumed in the combustion channel than should be required.

Table 3.1 Summary of enthalpy change in both channels under experimental conditions demonstrating the extensive heat loss compared to the theoretical combustion requirements

	Moles H_2 per mole CH_4	Inlet (kJ)	Outlet (kJ)	Difference (kJ)
Comb. Channel (Experimental)	36	+2950	-5480	-8430
Ref. Channel (Experimental)	1	8	170	162
Comb. Channel (Theoretical)	0.69	57	-105	-162

3.3.4 Effect of S/C on Reforming Fuel Conversion and H_2 Selectivity

As discussed previously, hydrogen selectivity varies between 0.75 and 1.00 and is dependent upon the reactant steam to carbon ratio (S/C) as well as the surface and exit gas-phase temperatures which affect the equilibrium concentrations determined by the water-gas-shift reaction (Equation 1.7). Figure 3.4 shows the relationship between reforming product H_2 selectivity and steam to carbon ratio.

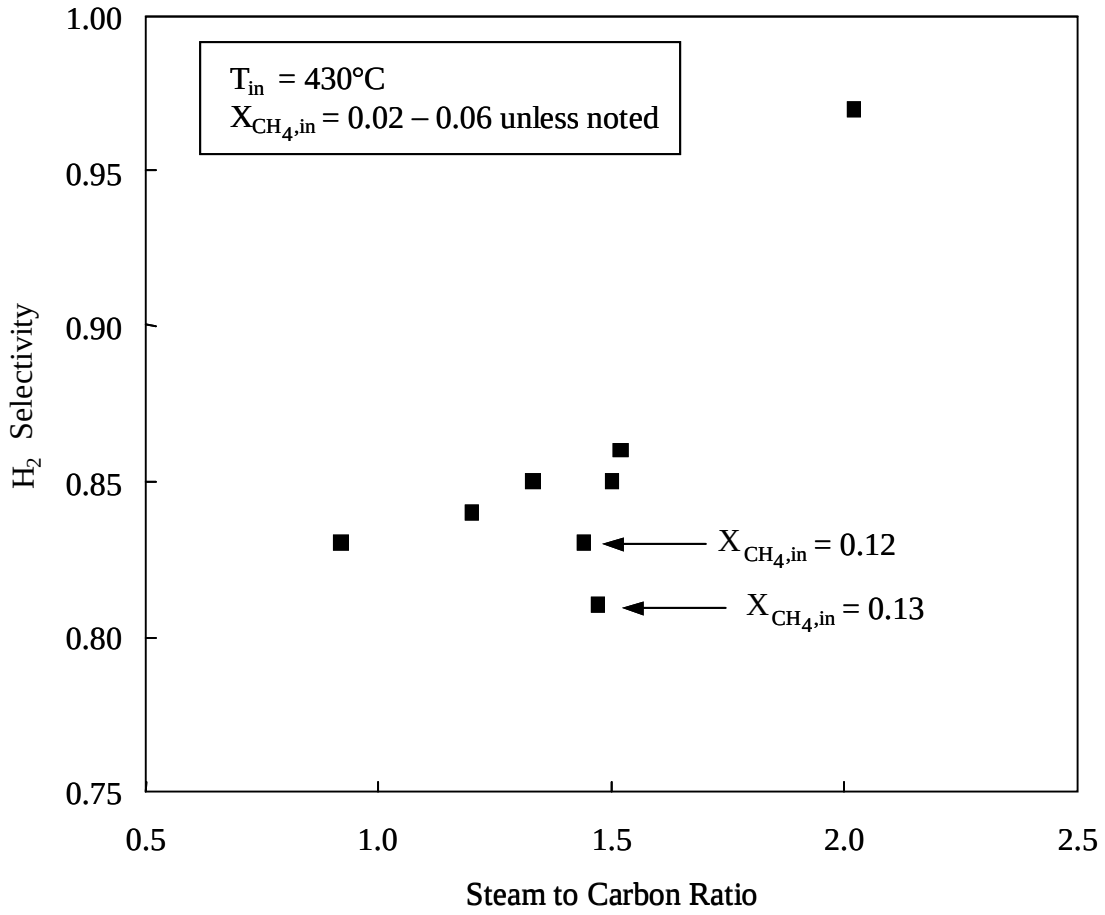

Figure 3.4 Plot of H_2 selectivity versus reforming steam to carbon ratio showing an expected rise in H_2 selectivity with increasing S/C

As expected, when S/C reaches 2.0, the selectivity should approach unity. For S/C values close to 1.5, indicating a process which produces nearly equal moles of CO

and CO_2, selectivity equals 0.87. When S/C drops below 1.5, the reaction converts the carbon to predominantly CO. The inability of the system to register this switch at low steam to carbon ratios demonstrates the likely presence of air leaks which impact the measurement of CO.

Surface temperature was found to be a determining factor for H_2 selectivity. Although surface temperature data is not available for these cases in Figure 3.4, the two points with the largest reforming fuel mole fractions (X_{CH_4} = 0.12 and 0.13) should produce cooler surface temperatures. As discussed in more detail in Chapter 5, the key reaction for determining the effectiveness for Rh catalysts is the two-step dissociative adsorption of methane on vacant Rh sites:

$$CH_4 + Rh(s) \rightarrow Rh\text{-}CH_4(s) \qquad 3.9$$

$$Rh\text{-}CH_4(s) + Rh(s) \rightarrow Rh\text{-}CH_3(s) + Rh\text{-}H(s) \qquad 3.10$$

Lower temperatures will limit the availability of vacant sites and thus reduce the conversion and selectivity.

To study the performance of the reformer independently of the combustor, several cases were run without combustion, relying solely on the furnace to supply the heat required for the reforming reaction. For these cases, the furnace was maintained at 750°C, while the reforming flow rate and steam to carbon ratio were varied. Figure 3.5a shows that H_2 selectivity is less dependent on residence time than conversion (which is

shown in Figure 3.5b). Figure 3.5a also shows the expected increasing trend in selectivity with increasing S/C.

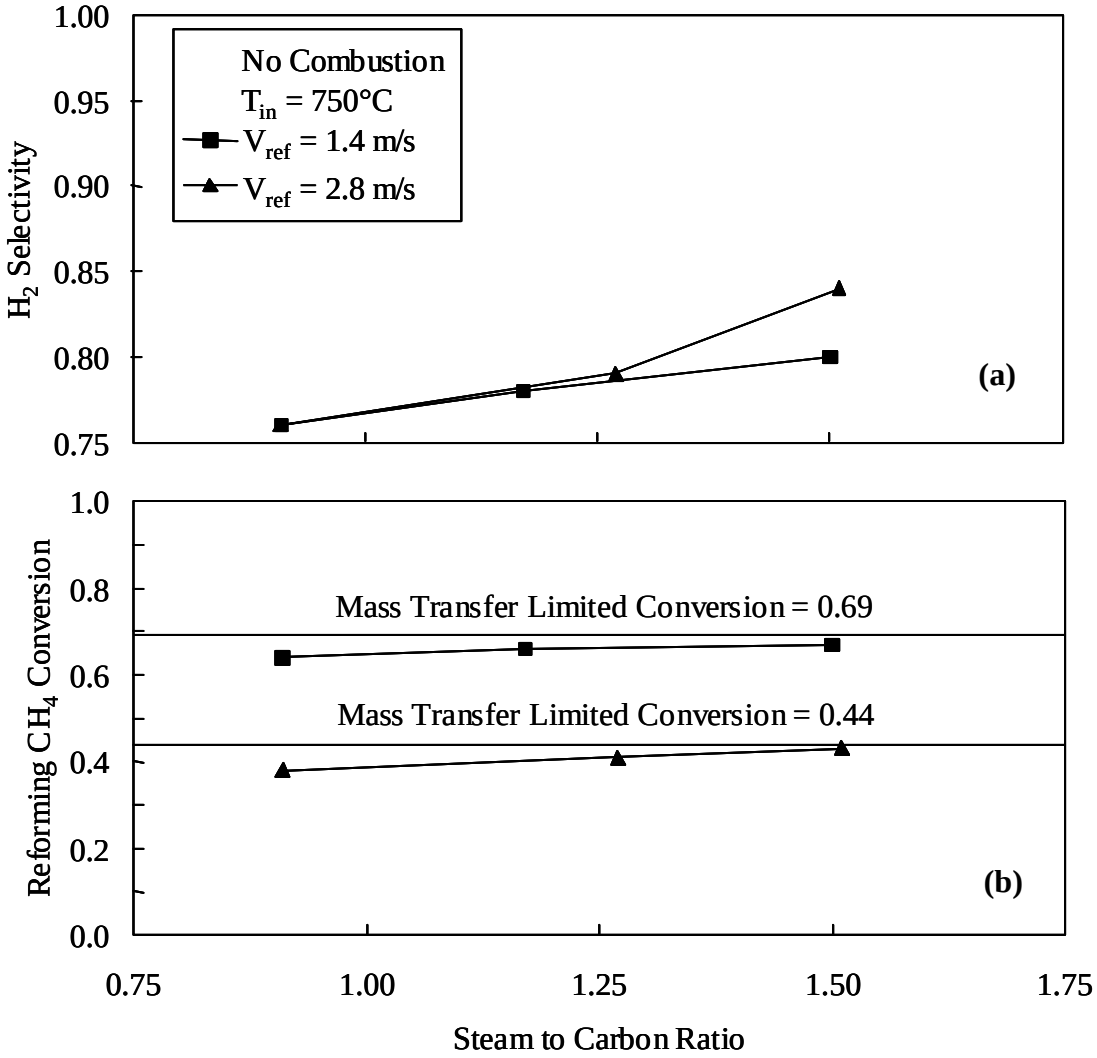

Figure 3.5 Results from reforming-only at elevated temperature (a) H_2 selectivity and (b) CH_4 conversion vs. S/C, including mass transfer limited cases

The mass transfer limited conversion for steam reforming can be approximated using a binary diffusivity for CH_4 in Ar calculated to be 1.77×10^{-5} using the Chapman-Enskog method (Turns 2000). For the conditions shown in Figure 3.5, the mass transfer limited conversions for u = 1.4 m/s and 2.8 m/s are 0.69 and 0.44, respectively. Figure 3.5b shows that the reaction is proceeding close to a mass transfer limited condition.

Chapter 4

Model Description

4.1 INTRODUCTION

This chapter discusses the adaptation of a single channel flow model (Zhu 2001) to accommodate the alternating two-channel configuration proposed in this study. This model combines two single channel models with a finite volume heat transfer model for the separating wall. Each channel flow model includes a porous washcoat model with independent gas phase and surface chemistry mechanisms. The time scales of the process, which can be on the order of minutes, require the channel models to be sufficiently fast to capture relatively slow transitions to steady state solutions. To this end, a transient quasi-one-dimensional formulation has been implemented for each channel flow where heat and mass transfer correlations determine gradients in temperature and species concentrations between the channel and respective washcoats.

4.2 CHANNEL FLOW MODEL

The model solves the one-dimensional transient governing equations for gas phase fluid flow with chemical reactions. The current model simplifies the governing equations reported in the previous model (Zhu 2001) by assuming negligible axial heat and mass diffusion in the gas phase as well as isobaric conditions. These assumptions

have a negligible impact on species concentrations and temperature profiles and the isobaric assumption enabled faster integration by avoiding the limitations of the compressible flow equations. Equation 4.1 presents the transient differential equation for species concentration in the channel flow:

$$\rho_g \frac{dY_{k,g}}{dt} = -a_{ch}\left(\rho_{gm} YV_{k,g} + \rho_{gm} V_g \left(Y_{k,gs} - Y_{k,g}\right)\right) + \rho_g u_g \frac{dY_{k,g}}{dx} + W_k \omega_{k,g} \qquad 4.1$$

where ρ_g is the gas-phase density, $Y_{k,g}$ is the gas-phase species mass fraction of species k, $YV_{k,g}$ is the mass-weighted diffusion velocity of species k, V is the average Stefan velocity from the washcoat to the channel due to gas-phase expansion, u is the mean axial velocity in the channel, a_{ch} is a geometrical factor for the channel, W_k is the species molecular weight, and ω_k is the molar production rate of the gas-phase species.

Equation 4.1 accounts for the mass transport between the channel and washcoat, mass transport via convection along the channel axially, and production due to gas phase chemical reactions within the channel. Gas phase chemical reactions for the conditions in this study (particularly the near atmospheric pressure condition) were found to have a negligible impact and thus the reactions were subsequently removed to decrease the integration time. In the above Equation 4.1, the mass weighted diffusion velocity of species k from the channel to the washcoat is shown:

$$YV_{k,g} = \frac{Sh_k D_k}{d_{hyd} W_{gm}} \left(\left(Y_{k,g} W_k - Y_{k,gs} W_k\right) + \frac{\Theta_k^T W_k}{T_{gm}} \left(T_g - T_{gs}\right) \right) \qquad 4.2$$

Where D_k is the multi-component diffusion coefficient, d_{hyd} is the hydraulic diameter, Sh_k is the Sherwood number for species mass transfer, Θ^T is the thermal diffusion coefficient,

T_g is the temperature gas in the channel, and T_{gs} is the temperature of the gas in the washcoat.

Equation 4.3 presents the transient temperature in the channel flow:

$$\rho_g C_{P,g} \frac{dT_g}{dt} = -a_{ch} h_T \left(T_g - T_s\right) - a_{ch} \rho_{gm} \sum_k \left(\left(h_{k,gm} - h_{k,gs}\right) Y V_{k,g}\right) + \rho_g u_g \frac{d\left(\sum_k \left(h_{k,g} Y_{k,g}\right)\right)}{dx} - \sum_k \left(W_k \omega_{k,g}\right) + a_{ch} \rho_{gm} V_g \sum_k \left(Y_{k,gm} \left(h_{k,gm} - h_{k,gs}\right)\right) \quad 4.3$$

Where $C_{P,g}$ is the molar specific heat capacity, h_T is the heat transfer coefficient, h_k is the species specific enthalpy, and x is the axial distance. Equation 4.3 accounts for convective heat transfer between the washcoat and channel, enthalpy changes due to mass transport, as well as convection along the channel axially.

The heat and mass transport between the channel and porous washcoat were handled using modified Graetz number heat and mass transfer correlations for reacting laminar flow based on a previous study (Groppi et al. 1995). The heat (h_T) and mass (h_K) transport coefficients were determined from calculating the Nusselt number (Eq. 4.4) and Sherwood number (Eq. 4.5).

$$Nu = \frac{h_T d_{hyd}}{\lambda_g} = Nu_1 + Nu_2 x_T^{Nu_3} \exp\left(-Nu_4 x_T\right) \qquad x_T = \frac{x u_{in} \rho_{g,in} C_{P,g,in}}{\lambda_{g,in}} \quad 4.4$$

$$Sh = \frac{h_K d_{hyd}}{D_k} = Sh_1 + Sh_2 x_k^{Sh_3} \exp\left(-Sh_4 x_k\right) \qquad x_k = \frac{x u_{in}}{D_{k,in}} \quad 4.5$$

The coefficients in the Equations 4.4 and 4.5 have been adapted for the parallel plate configuration and are given below.

$$Nu = Sh = 2.845 + 37.64\left(1000x^*\right)^{-0.350} \exp\left(-21.57x^*\right) \tag{4.6}$$

4.3 CATALYTIC WASHCOAT MODEL

Both the combustion and reforming catalytic washcoat layers have been modeled as a finite volume of a porous media with a set of transient differential equations governing the gas phase density and mass fractions as well as the surface and subsurface mole fractions. Uniform conditions were assumed within the washcoat in the direction normal to the catalytic surface. While the washcoat was discretized in the axial direction of the channel flow, the washcoat is considered uniform through its depth, which assumes no diffusion within this layer which may impact local gas phase mass fractions and consequently surface mole fractions. Equation 4.7 presents the transient differential equations for species concentration within the washcoat:

$$\begin{aligned}\varepsilon\rho_{gs}\frac{dY_{k,gs}}{dt} = a_{wc}\left(\rho_{gm}YV_{k,g} + \rho_{gm}V_g\left(Y_{k,gm} - Y_{k,gs}\right)\right) + \varepsilon W_k\dot{\omega}_{k,gs} + a_{cat}W_k\dot{s}_{k,gs} \\ - a_{cat}Y_{k,gs}\sum_k\left(W_k\dot{s}_{k,gs}\right)\end{aligned} \tag{4.7}$$

where ε is the washcoat porosity, a_{wc} and a_{cat} are washcoat and catalyst geometrical factors, and s_k is the molar production rate of species at the surface.

Similar to Equation 4.1 describing the channel flow, Equation 4.7 accounts for mass transport between the washcoat and channel, gas phase production within the

washcoat (although neglected in this study), and species production at the catalytic surface of the washcoat.

Equation 4.8 presents the transient temperature in the washcoat:

$$\overline{\rho C_{P,s}}\frac{dT_s}{dt} = a_{wc}h_T\left(T_g - T_s\right) + \frac{\lambda_s}{t_w}\left(T_{sav} - T_s\right) + a_{wc}\rho_{gm}\sum_k\left(\left(h_{k,gm} - h_{k,gs}\right)YV_{k,g}\right) + \left(v_{sub} + \varepsilon\right)\frac{d}{dx}\left(\lambda_s\left(\frac{dT_s}{dx}\right)\right) - \sum_k\left(a_{cat}W_k h_k \dot{s}_k + \varepsilon W_k h_{k,gs}\dot{\omega}_{k,gs}\right) + a_{wc}\rho_{gm}V_g\sum_k\left(Y_{k,gm}\left(h_{k,gm} - h_{k,gs}\right)\right) \quad 4.8$$

where T_s is the surface temperature, λ_s is the heat conduction, and v_{sub} is another geometrical factor. Also similarly to Equation 4.3 for the channel flow, Equation 4.8 accounts for convective heat transfer between the washcoat and channel, enthalpy changes due to mass transport, as well as convection along the channel axially. In the above equation the effective specific heat capacity for washcoat, substrate, catalyst, and gas in the washcoat is:

$$\overline{\rho C_{P,s}} = \varepsilon\rho_{gs}\Gamma_{cat}\sum_k\left(C_{Pk,gs}Y_{k,gs}\right) + a_{cat}\left(\Gamma_{cat}\sum_k\left(\overline{C}_{Pk,s}\theta_{k,s}\right) + \frac{\sigma_{cat}}{1-\sigma_{cat}}\sum_k\left(\overline{C}_{Pk,b}X_{k,b}\right)\right) + \left(1-\varepsilon\right)\rho_{wc}C_{P,wc} + v_{sub}\rho_{sub}C_{P,sub} \quad 4.9$$

In addition to these modes of heat exchange, the washcoat sub-model also includes axial heat conduction in the solid support. This term forces the set of equations to be second order PDE's. Lastly and critically for this dual channel reactor design, the washcoat model includes a conduction term through the shared support:

$$\frac{\lambda_s}{t_w}\left(T_{sav} - T_s\right) \quad 4.10$$

where t_w is half the thickness of the washcoat and support, T_{sav} is the average of the two surface temperatures, and T_s is the surface temperature of the respective channel.

The boundary conditions are at the reactor entrance for the species mass fractions, gas-phase and surface temperatures are given in Equation 4.11.

$$\begin{aligned} &\text{for } Y_{k,g} \quad Y_{k,g} = Y_{k,g,in} \\ &\text{for } T_g \quad \dot{m}\overline{C}_{P,g}\left(T_g - T_{g,in}\right) = \left(a_{sb} + a_{ch}\right)h_{T,in}\left(T_s - T_g\right) \\ &\text{for } T_s \quad \left(a_{sb} + a_{ch}\right)h_{T,in}\left(T_s - T_g\right) = \left(a_{sb} + a_{ch}\right)\lambda_s\left(\frac{dT_s}{dx}\right) \end{aligned} \qquad 4.11$$

The species mass fractions are defined as the inlet mass fractions while the temperatures are determined based on estimated heat conduction to the upstream flow.

The second order nature of the washcoat temperature equation requires an additional boundary condition at the exit of the reactor to solve for the solid phase temperatures. Shown in Equation 4.12, the model assumes an adiabatic condition at the downstream end of the channel.

$$\text{for } T_s \quad \left(a_{sb} + a_{ch}\right)h_{T,in}\left(T_s - T_g\right) = \left(a_{sb} + a_{ch}\right)\lambda_s\left(\frac{dT_s}{dx}\right) \qquad 4.12$$

4.4 SURFACE AND GAS PHASE CHEMISTRY

The catalytic combustion channel employs a preliminary Pd-H_2-CH_4-O_2 for supported polycrystalline Pd catalysts. This mechanism includes 35 elementary reaction steps involving 10 surface species and 2 subsurface species PdO(bulk) and reduced Pd(bulk). This mechanism has undergone preliminary validation (Zhu 2001) and has been shown to track the hysteresis of PdO_x reduction/oxidation cycles (Farrauto, Hobson et al. 1992).

There remains uncertainty regarding CH_4 steam reforming over transition metal catalysts. The current study has adapted a validated CH_4 partial oxidation mechanism over Rh catalyst (Schwiedernoch, Tischer et al. 2003). The mechanism has been modified to ensure thermodynamic consistency which requires that the activation energy for the reverse reactions are determined by balancing the enthalpies of formation for the reactants and products. Also, to accommodate the adsorption of water observed in the steam reforming experiments the initial sticking coefficient for H_2O was increased from 0.1 to 0.5. The sticking coefficient describes the probability that a species will adsorb onto the surface following a collision and ranges from 0 to 1. The resulting mechanism includes 38 elementary reaction steps involving 12 surface species.

For both the reforming and combustion mechanisms, the surface chemistry rate expressions were handled with Surface CHEMKIN (Coltrin et al. 1996). As mentioned earlier, for the conditions in the current study, it was found that the gas phase reactions in the washcoat and channel flow had a negligible impact on fuel conversion. Thus to increase the speed of the transient integration, the gas phase reactions were neglected and the gas phase species were limited to the reactants and major products which desorbed from the catalyst (CH_4, H_2, O_2, CO_2, H_2O, and N2 for the combustion mechanism and CH_4, H_2O, H_2, CO, CO_2, and Ar for the reforming mechanism).

4.5 NUMERICAL METHOD

The model combines the spatially discretized governing equations for both channels and washcoat layers into one vector of differential algebraic equations. This set of equations is integrated simultaneously using the stiff ODE solver LIMEX with a

maximum time step of 0.1s (Deuflhard et al. 1987). In order to capture radical changes in heat and mass transfer in the entry region, cell lengths at the front end of the reactor were limited to 0.1cm; however, a discretization study showed that cell lengths could be as large as 0.5 cm in the downstream portion of the reactor. Therefore, a variable grid size was used to save integration time when capturing long-term transients in this study. The variable grid used in this study to investigate a 10 cm long reactor is shown in Figure 4.1 and is defined as groupings of number of cells * cell size (cm):

2*0.1 2*0.2 18*0.5 2*0.2 = 10 cm

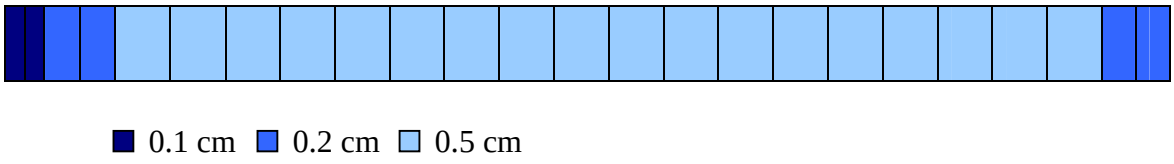

Figure 4.1 Variable grid used to investigate a 10 cm reactor indicating shorter cells at front of catalyst where the majority of the reactions occur

The model has its limitations. The implementation of heat and mass transfer correlations in lieu of 2-D channel flow models is what earned the model its "quasi" one-dimensional label. It is understood that a truly two-dimensional model would better capture the interaction between the two zones and has been explored elsewhere (Zhu 2001). In addition, the broad assumption of uniformity through the depth of the washcoat layer has recently been investigated to show that catalytic washcoat effectiveness does play a role in performance under conditions where the washcoat has thickness of 40 μm or more (Reihani et al. 2004). Effectiveness describes how the reaction rate through a non-uniform porous washcoat compares to a uniform one. However, in this study the washcoat thickness (~0.002 cm) is considered thin enough that the effectiveness is likely

near 1 and, therefore, a uniform washcoat assumption is a reasonable approximation. Lastly, because the purpose of this study is primarily to observe the trends in the dynamic relationship between the two reacting flows, a quasi-one-dimensional model is sufficient.

4.6 EXAMPLE BASELINE MODEL CASE

The model reports exit conditions of the reactor including gas-phase and surface temperatures, gas-phase mass fractions, and surface mole fractions as well as axial profiles of each parameter according to the grid discretization. The modeling analysis began by exploring the window of flow conditions that led to feasible reactor operating conditions. This led to a base case for the model simulations. The experimental efforts showed that, when using H_2 as the combustion fuel, setting T_{in} = 400 – 500°C and ϕ_{comb} = 0.3 – 0.4 was sufficient to sustain reforming reactions and suitable for observing changes in reactor performance. Therefore these conditions were chosen as the starting point for the modeling analysis. The steady-state axial profiles of surface temperature (T_s), combustion gas-phase temperature (T_g), fuel conversion, and the key surface mole fractions are in both channels shown in Figure 4.2. Figure 4.2 is included here as an example result, while a more detailed discussion on the significance of the shape of these profiles will be presented in Chapter 5.

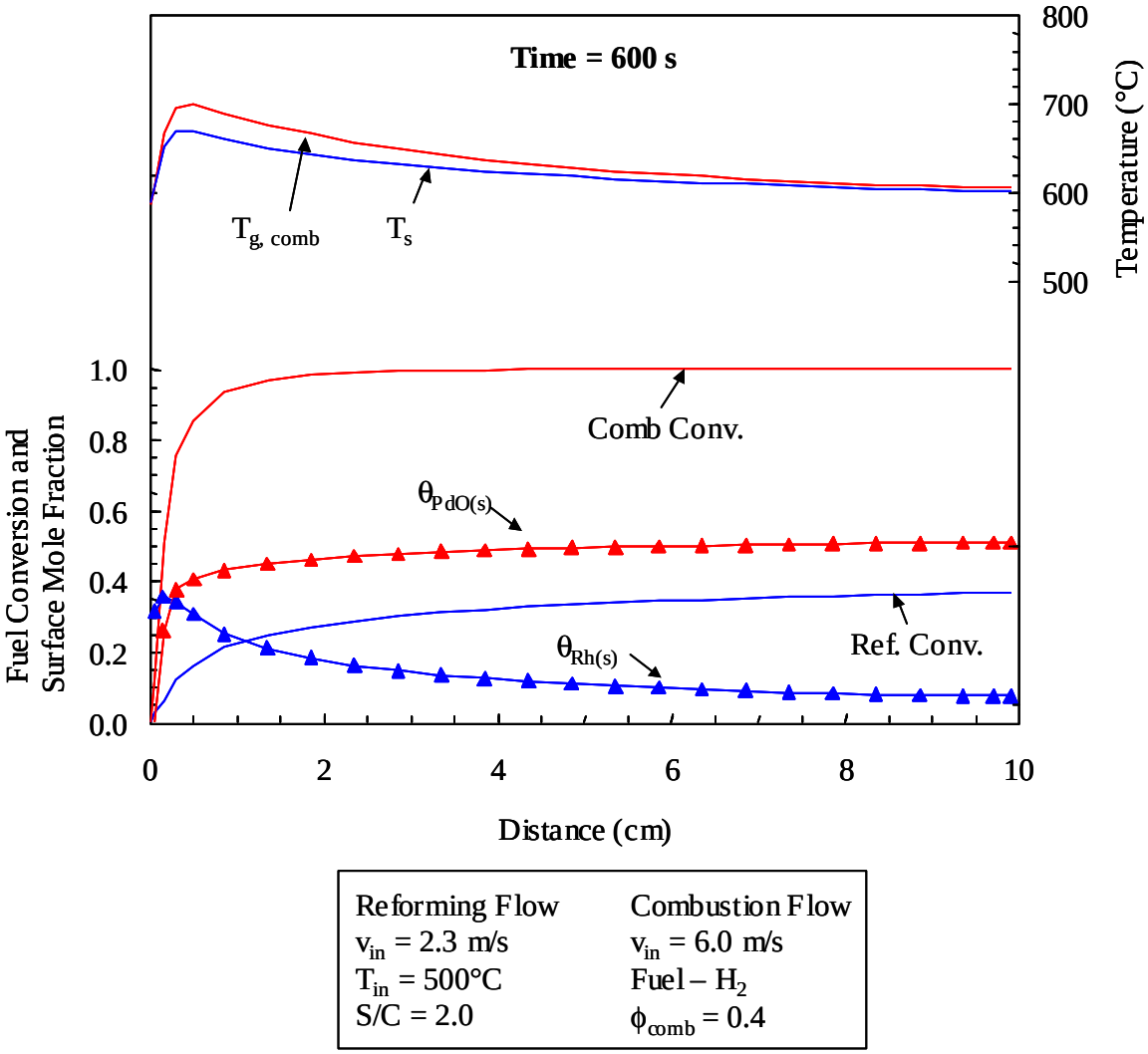

Figure 4.2 Example steady-state profile of baseline autothermal case modeling H_2 combustion over Pd catalyst and CH_4 steam reforming over Rh catalyst with T_{in} = 500°C, ϕ_{comb} = 0.4, and S/C = 2.0.

Chapter 5

Model Results

5.1 INTRODUCTION

Chapter 5 presents the results of the simulations conducted using the model described in Chapter 4. The model is first validated using the findings from the experiments. This validation shows the ability of the model to capture the steady-state performance over a range of conditions. Following this limited validation, the design of the simulated reactor will be extrapolated to a more realistic geometry and set of operating conditions. For all cases, the model was integrated for a simulated time up to t = 20 minutes by which time a steady-state condition had been achieved; however, steady-state conditions were often reached earlier than 20 minutes which the figures will reflect.

5.2 MODEL VALIDATION

Experimental data has been used to validate the model described in Chapter 4. Due to the extensive heat loss out of the reactor in the experiments which is not captured by the transient model, the model was modified such that the surface temperature profile could be fixed according to an experimental run when reliable temperature data was obtained. The steady-state performance of the reforming channel is then found numerically. Because the experiments were unable to produce accurate

results for both surface temperatures and exhaust gas analysis simultaneously, the steady-state numerical performance (found with the fixed surface temperature profile) must be compared to a separate experimental run which has been conducted with identical inlet conditions when reliable exhaust analysis data was obtainable. The comparison of the numerically derived and experimentally derived CH_4 conversion and H_2 selectivity are shown in Figure 5.1 and are indicated by the red lines. To demonstrate the motivation for the additional effort to validate the model, a scenario is also shown in Figure 5.1 which allows the model to calculate the surface temperature profile and is indicated by the blue lines.

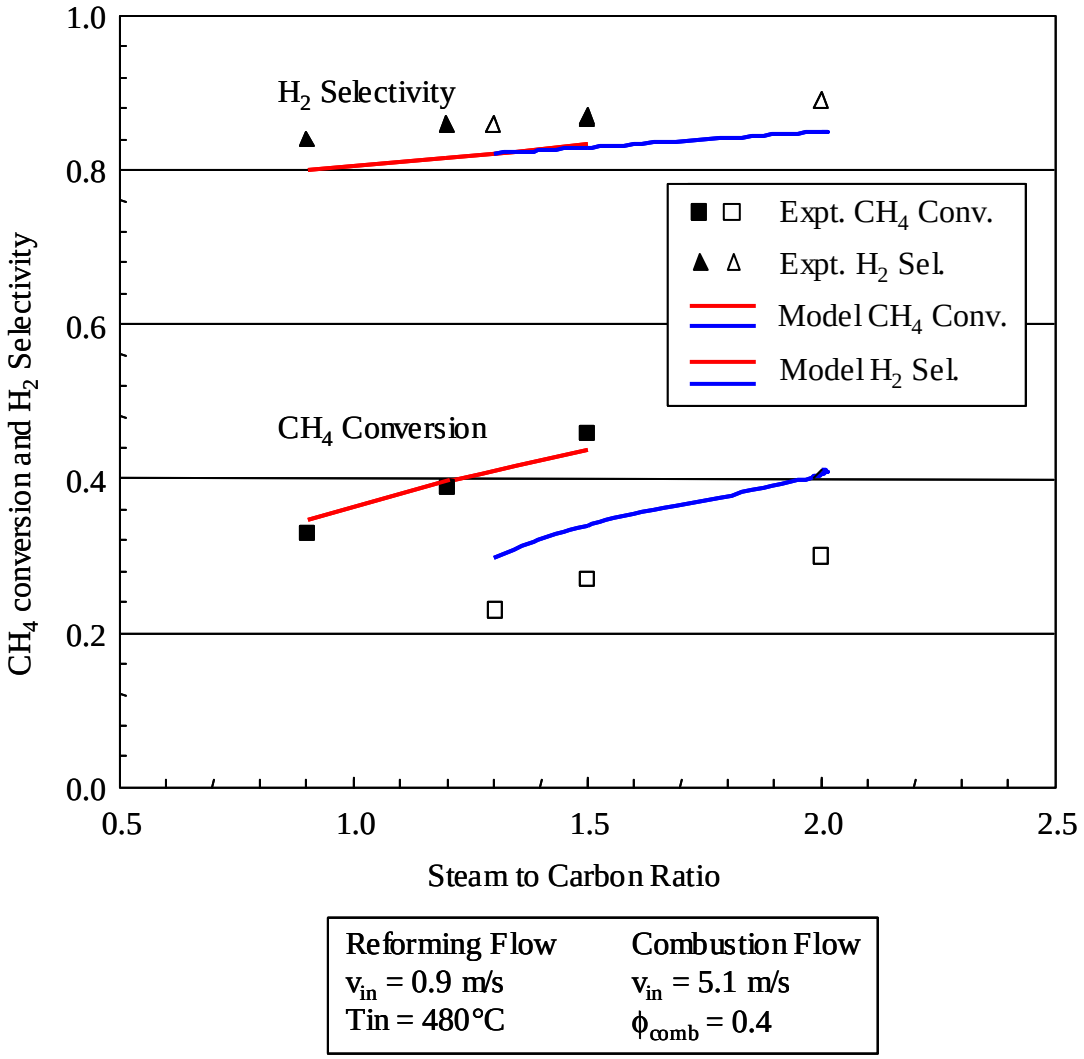

Figure 5.1 Comparison of experimental results using H_2 combustion with numerical model predictions for reforming CH_4 conversion and H_2 selectivity. Red lines indicate model predictions where experimental temperature profiles are input to the model and blue lines indicate model predictions where temperature profiles are solved by the model.

As expected, the model over predicts the conversion by assuming an adiabaticity that was not present in the experiments. From the comparisons presented in Figure 5.1, the model has been shown to be capable of capturing trends in catalyst performance for a range of steam to carbon ratios.

5.3 MODEL RESULTS

5.3.1 Reactor Design Extrapolation

Once the model had been validated by the experiments, the reforming flow rates and reactor geometrical parameters were adjusted to simulate a more realistic reactor design. The noteworthy changes between the experimental reactor and simulated reactor include nearly doubling the length from 5.5 cm to 10 cm, halving the thickness of the fecralloy substrate from 1.0 mm to 0.5 mm, and removing the diluent in the reforming channel. All of these changes are intended to investigate conditions expected in practical reforming applications. A summary of the model parameters and range of conditions studied here are presented in Table 5.1. These parameters do not necessarily represent optimum conditions with respect to efficient hydrogen production, but were found to provide reasonable performance for evaluating practical design applications. Optimization of the manifold parameters and conditions was beyond the scope of this study.

Table 5.1 Simulated experimental parameters used for modeling a single plate reactor with integral catalytic combustion/steam reforming

	Catalytic Combustion Channel	Steam Reforming Channel
Catalyst/support (1.0 mm thick Fecralloy for experiments, 0.5 mm otherwise)	0.6% Pd on 50% porous Al_2O_3 washcoat on a Fecralloy support	1.7% Rh on 50% porous Al_2O_3 washcoat on a Fecralloy support
Surface chemistry mechanism	(Zhu 2001)	(Schwiedernoch, Tischer et al. 2003)
Catalyst area/washcoat volume	3000 cm^{-1}	6000 cm^{-1}
Channel length	100 mm	100 mm
Height (between plate centers)	3.2 mm	3.2 mm
Washcoat thickness	0.025 mm	0.025mm
Inlet velocities	3.0 m/s, 6.0 m/s	6.0 m/s
Inlet composition	H_2 or CH_4, ϕ_{comb}: 0.2, 0.3, 0.4	H_2O/CH_4: 0.9-2.0 (for experimental cases), H_2O/CH_4: 1.3-2.0 (otherwise)
Diluent	N_2	Ar (for experimental cases only)
Inlet conditions	T_{in}=400-600°C, P=1atm	T_{in}=400-600°C, P=1atm
Initial catalyst conditions	PdO_x (surface and in bulk phase)	Rh (surface and in bulk phase)

The experiments were required to use a diluent to reduce the steam content of the reforming flow for analysis purposes; however, the diluent was removed in the model runs as it reduces the H_2 mole fraction in the reformate and would be absent in any real system. With the diluent removed, the system is designed to be run autothermally where the reforming channel uptakes all of the heat release from the combustion channel. The model analysis therefore carries the autothermal conditions as the baseline and investigates how deviations in either direction affect fuel conversion, H_2 selectivity, catalyst composition, and surface temperatures.

5.3.2 Effect of ϕ_{comb} on Autothermal Operation

Figure 5.2 shows how the model captures the transient catalytic ignition indicated by the surface temperature, T_s, and gas-phase temperature in the combustion channel, T_g, at the exit of the reactor. The gas-phase temperature in the reforming channel is not shown because it closely tracks the surface temperature (always within 2.5°C) due to the narrow channel height and rapid equilibration of the flow and surface.

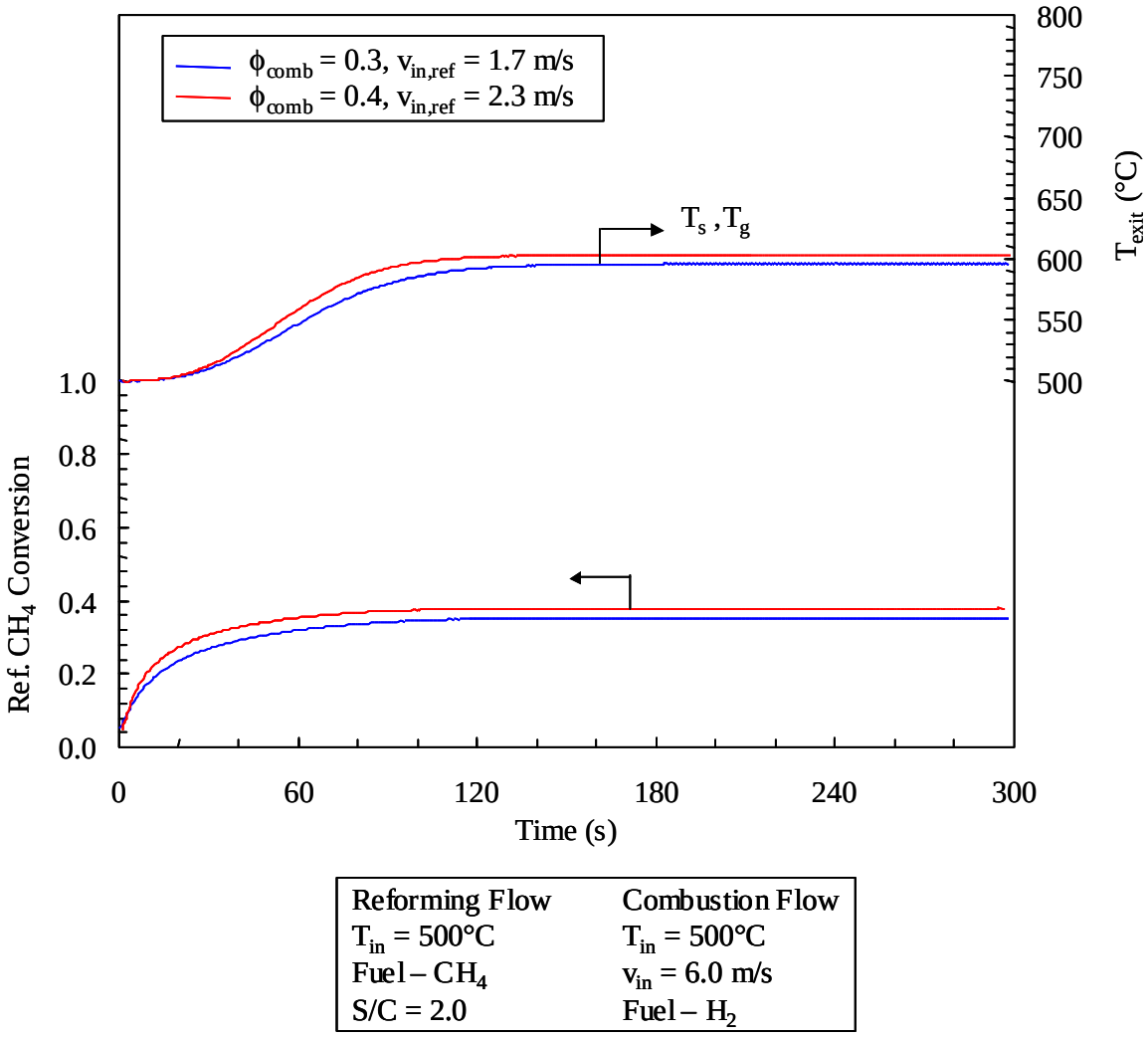

Figure 5.2 Plot of transient reformer fuel conversion and exit temperature demonstrating the small impact of ϕ_{comb} on autothermal operation

The cases shown in Figure 5.2 are nearly autothermal as the reforming velocity has been increased in response to the additional fuel content on the combustion side for ϕ_{comb} = 0.4. In each case, the exit reforming fuel conversion rises in time until the downstream plate temperature reaches an equilibrium between the heat released on the combustion side and the heat extracted by the reforming channel. The combustion fuel conversion is not included since it reaches full conversion >0.99 within the first 3 s of integration. Figure 5.2 indicates that ϕ_{comb} alone has a small impact on reforming fuel conversion when

autothermal conditions are satisfied; however, adjusting the ratio of the fuels in each channel will produce a noticeable change in performance.

5.3.3 Effect of Inlet Temperature on Steady-State Profiles of Temperature and Surface Mole Fractions

The activity of both the reforming and combustion catalysts is closely tied to surface temperatures along the reactor. Figure 5.3 plots the steady-state axial profiles of critical surface mole fractions where $\theta_{PdO(s)}$ represents palladium oxide sites in the combustion channel and $\theta_{Rh(s)}$ represents vacant rhodium sites in the reforming channel.

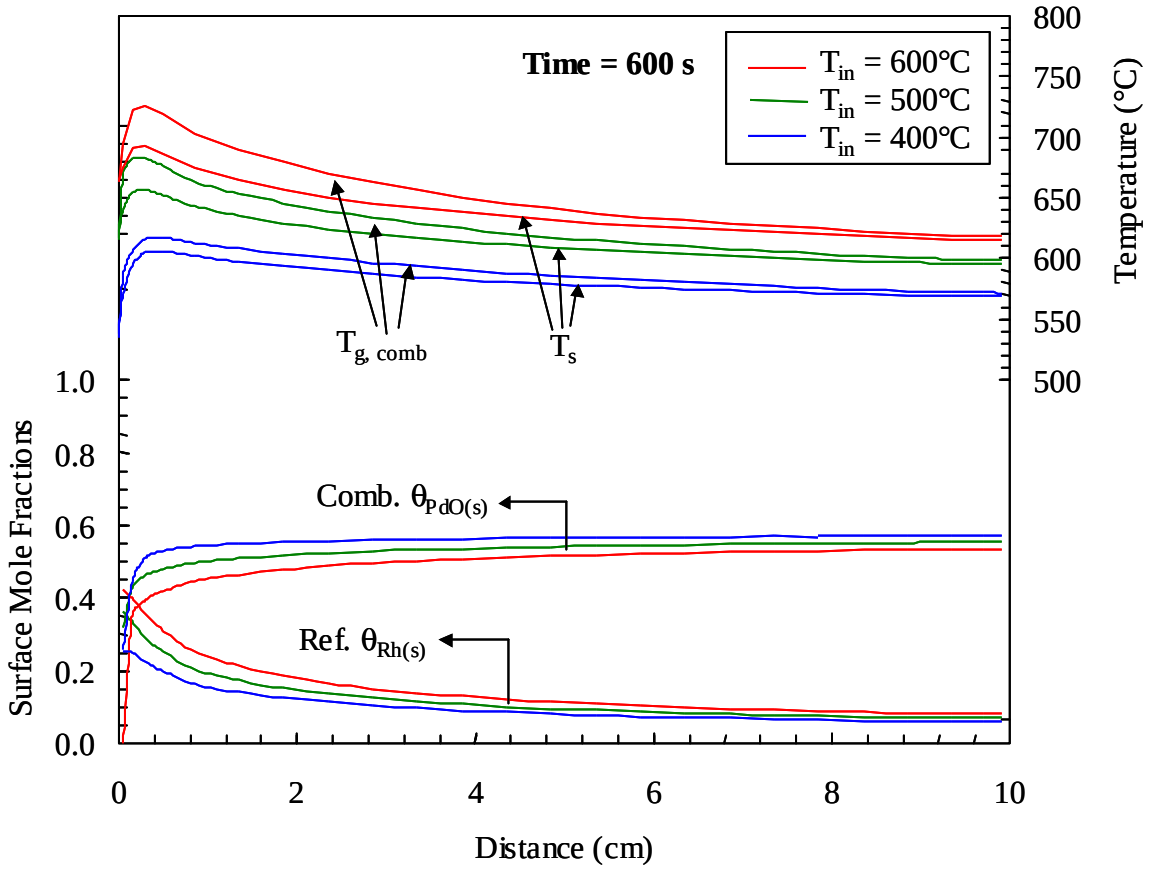

Reforming Flow	Combustion Flow
v_{in} = 1.7 m/s	v_{in} = 6.0 m/s
Fuel – CH_4	Fuel – H_2
S/C = 2.0	ϕ_{comb} = 0.3

Figure 5.3 Effect of T_{in} on steady-state profiles of critical surface site fractions in both channels on reactor temperature profiles

As touched on in Chapter 3, the controlling reactions in both channels involve the adsorption of the limiting reactant (CH_4 in reforming and H_2 for combustion). The two-step dissociative adsorption reaction of methane recalled from Equations 3.7 and 3.8 illustrates the importance of maintaining a high number of vacant Rhodium sites.

$$CH_4 + Rh(s) \rightarrow Rh\text{-}CH_4(s) \quad 3.7$$

$$Rh\text{-}CH_4(s) + Rh(s) \rightarrow Rh\text{-}CH_3(s) + Rh\text{-}H(s) \quad 3.8$$

The dissociative adsorption of hydrogen shown in Equation 5.1 actually occurs on a PdO(s)/Pd(s) (oxide/vacancy) pair which therefore implies that a balance of both palladium species is important. Up until the reduction temperature, the oxide species PdO(s) dominates the surface and the adsorption rate is therefore controlled by the vacancy site fraction.

$$H_2 + Pd(s) + PdO(s) \rightarrow PdO\text{-}H(s) + Pd\text{-}H(s) \quad 5.1$$

Figure 5.3 shows that rapid combustion in the extreme front end of the catalyst for all cases reduces the PdO(s) site fraction dramatically due to a rapid temperature rise above the PdO(s)→Pd(s) transition temperature. The highest surface temperatures occur immediately downstream of this reduction zone. These high surface temperatures are capable of keeping a high proportion of rhodium sites vacant and receptive to methane molecules. Further downstream, the rhodium sites become covered with carbon monoxide, Rh-CO(s) species, as surface temperatures are no longer sufficient to encourage the desorption of the reforming products. The lower inlet temperature cases exhibit this blocking of active sites earlier due to the lower surface temperatures

produced at the front end of the catalyst. Figure 5.3 shows that extending the reactor length is only effective if surface temperatures can be maintained at a level suitable for reforming.

5.3.4 Effect of Inlet Temperature on Steady-State Profiles of Temperature and Reforming Fuel Conversion during Sub-Autothermal Operation

As discussed in Figure 5.3, inlet temperature and more importantly initial surface temperature can play a significant role in establishing steady-state conversion. Lower inlet temperatures will rely heavily on the combustion to heat the catalyst support, thus reducing the portion of the fuel energy that can be translated to the reforming channel. Figure 5.4 plots transient conversion and exit temperatures for three different inlet temperatures.

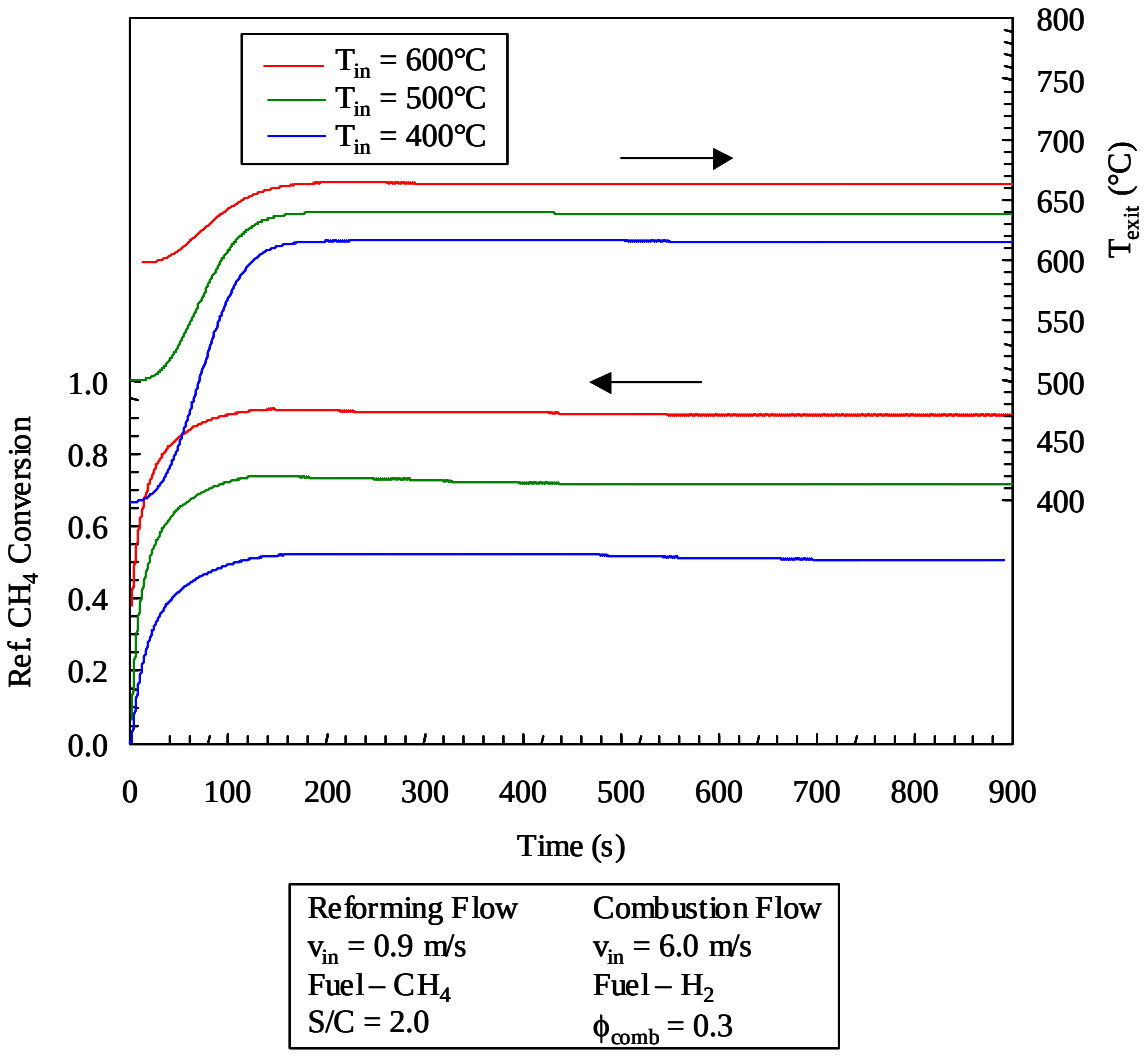

Figure 5.4 Transient profiles of conversion in reforming channel and exit temperatures for a range of T_{in} with excess combustion showing slight decay in conversion with time due to combustion catalyst reduction

The reforming flow rates shown in Figure 5.4 are considered sub-autothermal because they are too low to draw the heat away from the combustion channel as quickly as it is produced. This inability to absorb all of the combustion heat allows surface temperatures even for T_{in} = 400°C to rise sufficiently to permit significant reforming; however, the steady-state conversion is still roughly half that of T_{in} = 600°C. It is worth noting that the T_{in} = 400°C case actually sees a large change in exit temperature than the

T_{in} = 600°C case. The higher inlet temperatures produce higher reforming rates early in the process which limit the change in front end temperatures. This trend confirms that surface temperature is a prime indication of the conversion and further explains why the model was more successful at matching experimental conversion when the experimental surface temperature profile was implemented.

5.3.5 Effect of Reforming Flow Rate on Steady-State Profiles of Temperature and Reforming Fuel Conversion

All of the analysis presented thus far points towards the ratio of the flow rates, or the extent to which the process is autothermal, as the variable that is a primary determinant of the surface temperature and final conversion. The effect of reforming flow rate on steady-state conversion is summarized in Figure 5.5. The autothermal rate (1.13 moles of H_2 fed to the combustor per mole of CH_4 to the reformer) is compared to twice (0.57) and half (2.26) the autothermal rate.

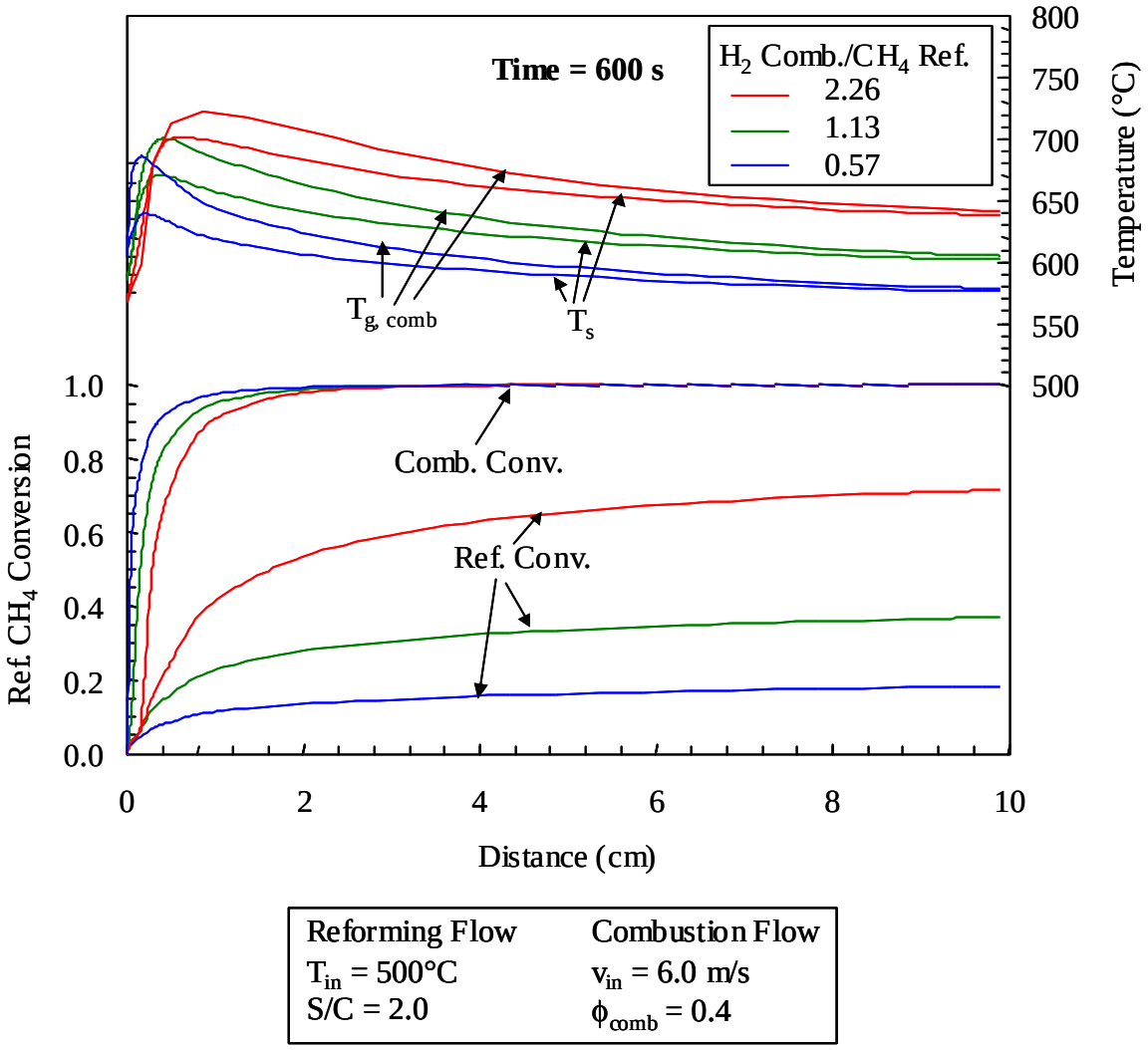

Figure 5.5 Effect of reforming flow rate on steady-state CH_4 conversion in the reforming channel and on reactor temperature profiles

For each case in Figure 5.5, the combustion channel reaches full conversion near the entrance of the reactor so the impact on surface temperatures and reforming fuel conversion resides with the ratio of the flow rates. Higher reforming flow rates mitigate surface temperatures resulting in a drop in conversion. Sub-autothermal flow rates allow temperatures to rise well above 600°C along the length of the reactor and boost conversion

5.3.6 Effect of Combustion Fuel Selection on Steady-State Profiles of Temperature and Reforming Fuel Conversion

The combustion surface chemistry mechanism was developed to capture the complete oxidation of CH_4, which includes the oxidation of H_2 species. The integrated reformer system was envisioned to use CH_4, H_2 or a combination of fuels for the combustion heat source depending on the application. Figure 5.6 shows the steady-state profile of fuel conversion in both the combustion and reforming channels and illustrates the differences between a system using an H_2-fueled combustor and one that is fueled by CH_4.

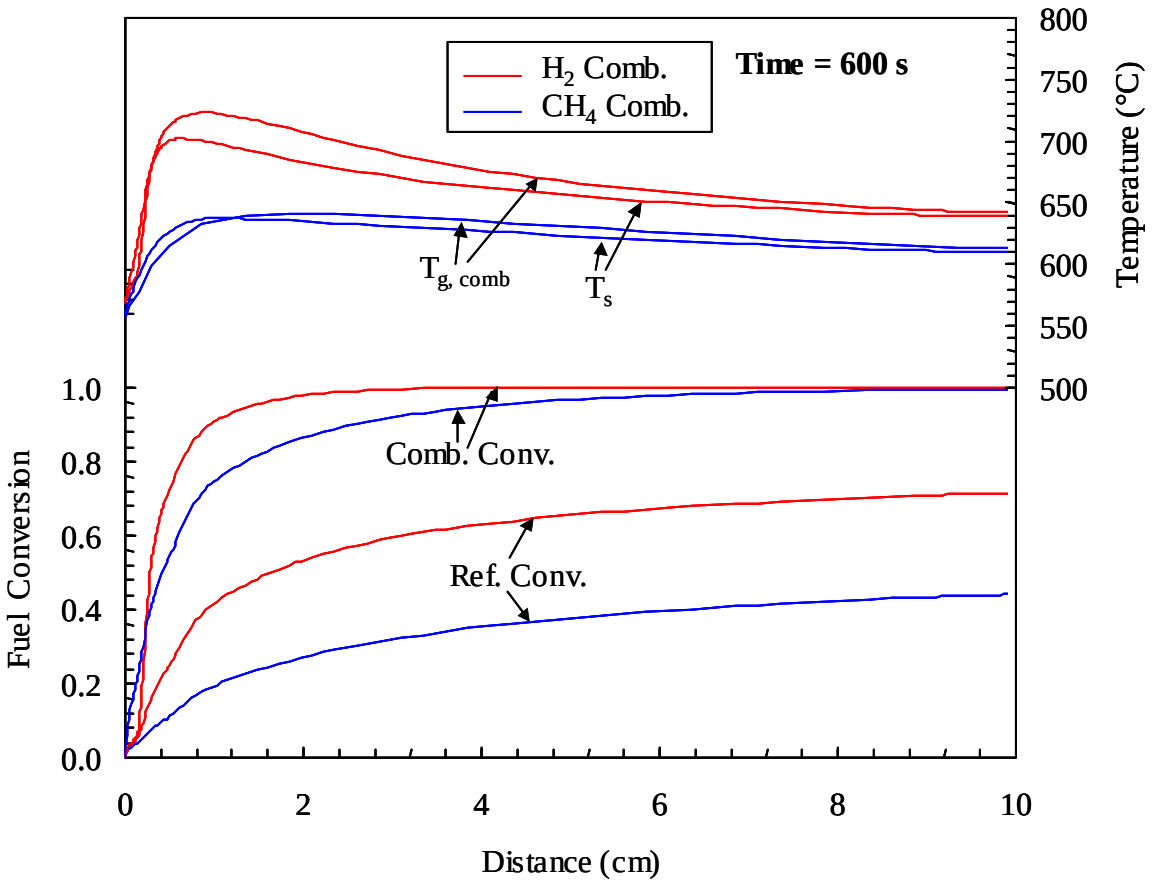

Reforming Flow	Combustion Flow
v_{in} = 1.15 m/s	v_{in} = 6.0 m/s
T_{in} = 500°C	Fuel – H_2 , CH_4
S/C = 2.0	ϕ_{comb} = 0.4

Figure 5.6 Steady-state conversion and temperature profiles illustrating the differences between H_2-fueled and CH_4-fueled combustion

The rapid temperature rise of H_2 combustion with respect to CH_4 combustion promotes higher rates of reforming and reforming fuel conversion. This rapid temperature rise with H_2 combustion has also been reported in literature (Hegedus 1975). Although all of the combustion fuel for both systems is consumed by the end of the reactor, the H_2-fueled system is able to achieve higher surface temperatures downstream which are critical for high reforming conversion. Another point worth noting is that, for

the conditions shown in Figure 5.6, the extreme front end of the catalyst (0.2 cm) has been reduced; however, the H_2-fueled combustor has overcome this drop in activity due to the fact that H_2 mass diffusion to the surface is faster than the thermal diffusion away from the surface, i.e. H_2 has Lewis number <1.

5.3.7 Effect of the Ratio of Fuel Burned to Fuel Reformed on Steady-State Reforming Fuel Conversion over a Range of Inlet Temperatures

Several model cases have been run to compare the performance of the reformer using H_2 and CH_4 as the combustion fuel over a range of inlet temperatures. The results of these model runs are shown in Figure 5.7. In order to plot both fuels on the same scale, the moles of H_2 burned were divided by 4.0 to reflect an equivalent O_2 consumption compared to CH_4 combustion.

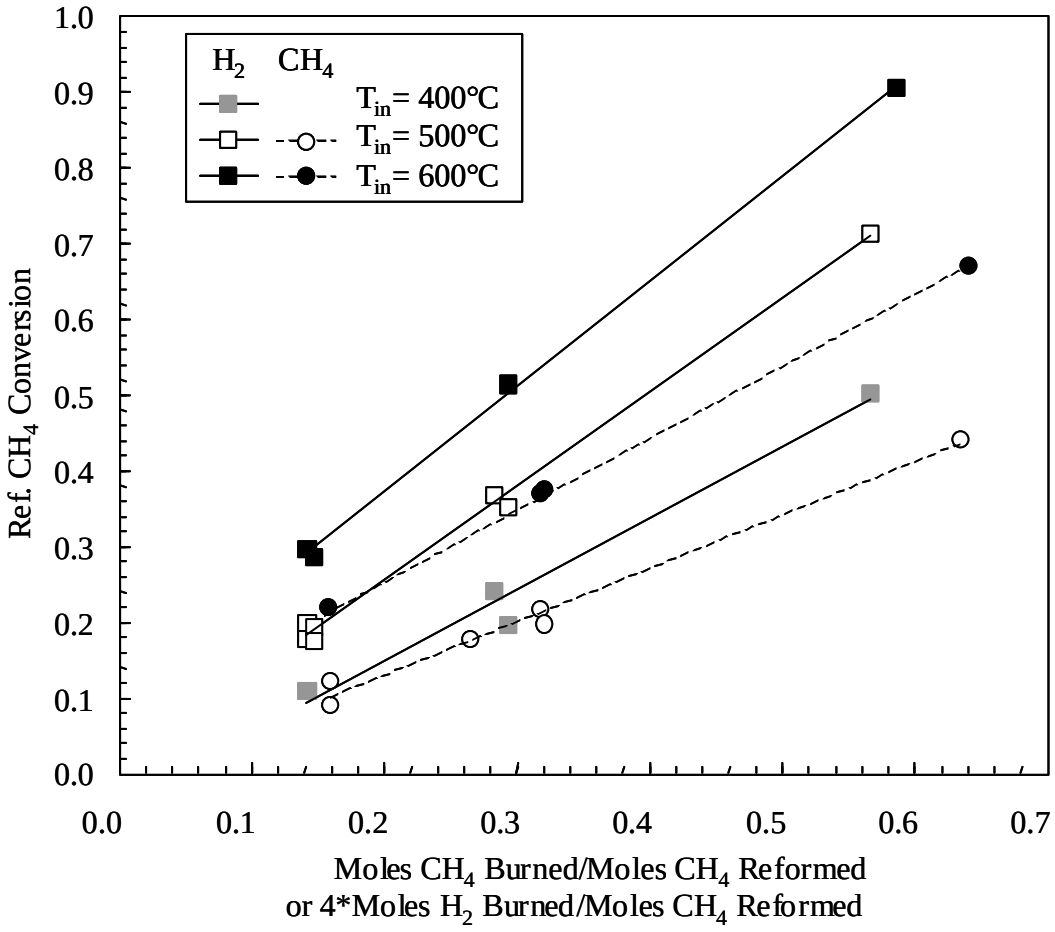

Figure 5.7 Plot showing reforming CH_4 conversion as a function of the ratio of moles of fuel to the combustor to moles of fuel to the reformer for a range of T_{in}

The linear relationship between the reforming fuel conversion and ratio of moles burned to moles reformed is unexpected. Figure 5.7 shows an anticipated improvement in conversion with H_2 as the combustion fuel likely due to the resulting higher surface temperatures for a given set of inlet conditions. Figure 5.7 points out the lack of adiabaticity present in the experiments. It has been shown that the majority of reforming conversion is done in the front half of the reactor. Therefore the exit conversions reported in Figure 5.7 indicate that nearly 30 times more fuel was necessarily burned in the experimental reactor (Figure 3.3) to match the adiabatic results in this study. A portion of this additional fuel can be attributed to the increased wall thickness of the

experimental reactor (1mm) compared to the model (0.5mm) and associated increase in heat conduction out the sides of the substrate.

5.3.8 Effect of Reformer Exit Temperature on H_2 Selectivity

Since the surface chemistry mechanism for steam reforimng was principally adopted from a partial oxidation mechanism, the model is less successful, with respect to conversion, at quantitatively capturing the H_2 selectivity in the reformate. Nevertheless, the model results show the trends one would expect for how the steam to carbon ratio in the reforming channel and reformer exit temperature affect H_2 selectivity.

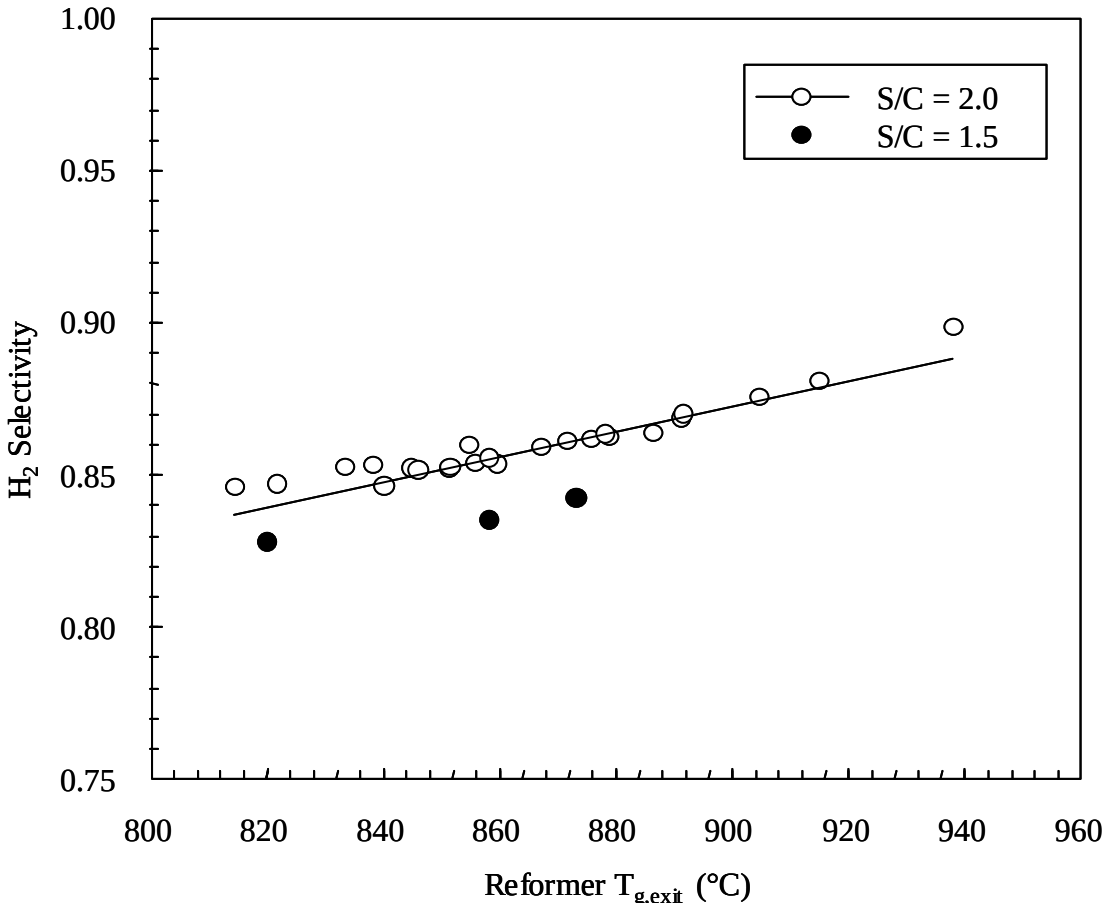

Figure 5.8 Plot of reformer H_2 selectivity as a function of exit gas-phase temperature

Figure 5.8 shows the expected increase in H_2 selectivity for cases with a steam to carbon ratio of 2.0 compared to 1.5. The additional steam and higher reformate temperatures drive the water-gas-shift equilibrium toward H_2 and CO_2. The positive slope of the line in Figure 5.8 indicates that the process is still approaching equilibrium. The scatter in the model results in Figure 5.8 is due to slight variations in some of the input parameters, such as T_{in}, ϕ_{comb}, and inlet velocities.

Chapter 6

Conclusions and Future Work

6.1 CONCLUSIONS

The current work has proposed a novel reactor design for efficient hydrogen production where catalytic combustion of either H_2 or CH_4 produces the necessary heat to drive CH_4 steam reforming occurring on the opposite side of a shared surface. This concept was investigated both experimentally and numerically by examining the dynamic relationship between just two channels of an overall multi-channel reactor.

In the experimental portion, a setup was devised to study the effect that steam content, inlet temperature, combustion fuel to reforming fuel ratio, and inlet velocity had on reforming fuel conversion and hydrogen selectivity. Most significantly, this work sought to gain a level of understanding, which to this point has been absent from the reported literature, about the complex and changeable nature of the surface chemistry occurring within both channels. To this end, the experiments measured surface temperatures along the catalytic region while simultaneously measuring the reformate exhaust in order to capture the transients of such a process. The surface temperature measurements, though extremely challenging to obtain, indicated the location where the principal reforming occurred and demonstrated the ability of the reforming to mitigate the combustion temperatures in order to keep the palladium catalyst in an active oxidized state. The experiments also showed that by raising the heat input to the system, either by

raising the inlet temperature or increasing the moles of fuel fed to the combustor relative to the moles of fuel fed to the reformer, the conversion and selectivity increased.

The knowledge gained from the experiments was then applied to a transient dual channel model which incorporated two separate detailed surface chemistry mechanisms and the heat exchange across the shared surface. The heat loss in the experiments and the inability to consistently measure both temperatures and conversion made a strong validation difficult to achieve. The level of validation, however, was sufficient to justify using the model for studying qualitative effects that operating conditions would have on the performance of a more realistic reactor. Model results showed that reactor performance depends greatly upon maintaining a hot but active catalytic surface. For effective steam reforming, the surface temperature must be maintained above 600°C. Inlet temperature, combustion equivalence ratio ϕ_{comb}, and reforming flow rates all affect the surface temperature. Ideally, the reactor is to be operated autothermally where all of the heat release produced is consumed by the endothermic steam reforming reactions. This situation generates the highest amount of hydrogen for a given flow rate. When reforming flow rates are greater than autothermal, inlet temperatures must be held high to sustain the reforming reactions. However, when reforming flow rates are sub-autothermal, even low inlet temperatures ~400°C are sufficient to allow front end temperatures to rise suitably to allow moderate reforming.

The current work also compared the performance of a reactor relying on CH_4 as the combustion fuel instead of H_2. In the experiments, CH_4 was initially used as the combustion fuel, but it was unable to sustain surface temperatures above 600°C without inlet temperatures above 500°C due to the heat loss through the reactor walls.

Numerically, CH_4 was found to be less effective than H_2 at maintaining the surface temperatures and that, for a given fuel stoichiometry, H_2 fueled combustion resulted in higher reforming rates and increased reforming fuel conversion.

The work, principally in the experiments, presented several challenges. A large portion of the experimental effort was focused on determining a window of stable operation where the combustion reactions could sustain the reforming. This proved difficult because CH_4 could not raise the surface temperatures rapidly enough, and so H_2 was substituted as the combustion fuel. With H_2 as the fuel, the combustion side was prone to autoignition in the mixing zone. Measures were taken to remove dead zones in the reactor, but it was ultimately found that the inlet temperature must be kept below 450°C and ϕ_{comb} below 0.4 with H_2 as the combustion fuel. The restriction on these inlet conditions placed additional limitations on the maximum surface temperatures achievable and thus narrowed the window of exploration further.

Another significant challenge was the use of the quadrupole mass spectrometer to measure the concentrations of the products in the reformate exhaust. A mass spectrometer was selected as the principal analysis tool because the prime objective of this work was to study the transient behavior of the process. A gas chromatograph, or GC, is often used in reforming studies, but the long lag times inherent in its operation preclude it from capturing transients. It is therefore usually used for steady-state measurements. Being a vacuum system, the mass spectrometer responds slowly to water, which will stick to the inner walls of the vacuum chamber and detector and disrupt the measurements. As its name implies, steam reforming contains a significant amount of moisture. The reforming conditions were therefore tailored to be heavily diluted so that

the effects of the residual steam could be processed out during the analysis. The heavy dilution, coupled with the heat loss in the reactor, prevented operating the reactor autothermally.

A last major challenge in the experiments was measuring the surface temperatures, which were again crucial for achieving the work's objective of studying the transient development of the catalytic ignition along the surface and the response to the reforming reactions. When to attach the thermocouples to the Fecralloy plate presented its own challenges. It was determined that the readings would be most accurate if the thermocouples were attached prior to catalyst coating. However, to prepare the Fecralloy plate for coating, the plate was oxidized at 1100°C in a muffle furnace which would push the bare wire K-type thermocouples to their maximum service limitations even before use. Higher temperature R-type thermocouples were explored, but they were still difficult to run out of the oxidizing furnace and due to their precious metal content, R-type thermocouple measurements are influenced by catalytic reactions on the bead surface. Ultimately, the solution was to tack the TCs after coating by removing just enough catalyst to allow the thermocouple bead to contact the surface. Once the thermocouples were attached, running them out of the reactor proved difficult. The bare wire thermocouples were sheathed in high temperature ceramic to keep them isolated. This ceramic sheathing required that the gasket material supporting the Fecralloy plate and forming the reaction channels be pliable enough to seal around the thermocouples. In the end, it was determined that the seal was never good enough to prevent all leaks into the reactor. As a result, there existed a trade-off between measuring accurate temperatures and reforming product concentrations. Experimental cases were therefore

run where either one but not both forms of data were considered reliable. Separate cases were run using similar inlet conditions in attempt to match reliable temperature data with reliable product concentrations.

Answering all of the challenges presented by the experiments and still coming away with meaningful data which could be used to validate the steady-state output of a numerical model was in itself satisfying. The appreciation of numerical tools and the experimental process and the ability to identify and work within the limitations of each are the most significant personal outcomes of this research.

6.2 RECOMMENDATIONS FOR FUTURE WORK

The numerical and experimental findings of this research demonstrate that there is both a need and reason for continuing the current work. Alternative energy remains a buzz word in the national agenda, and hydrogen consuming fuel cells for both stationary and transport applications continue to receive a lot of attention and funding. Until a nuclear based source of hydrogen production is implemented, reforming remains one of only a few economically viable solutions to providing an on-site hydrogen rich effluent from a variety of fuels.

The reforming experiments could be revisited with improved diagnostics. Surface temperature measurements would need to be made perhaps with remote IR measurements through an optical port such that the measurements do not interfere with the reactor operation or other data collection. Improvements in thermal management would enable the use of CH_4 as the combustion fuel which could eliminate much of the pre-ignition

problems of the H_2 fed combustor. The problems associated with the reformate exhaust analysis must be addressed. If a mass spectrometer is to be used to capture transients then the reformate moisture must be removed, perhaps using a desiccant system, prior to entering the detector. Separate CO and CO_2 measuring tools would improve the accuracy of conversion and selectivity data.

Numerical model validation would benefit from the improvements made to the experiments described in this work as well as additional surface catalysis research. The understanding of lean combustion of CH_4 over PdO_x is continually being improved upon; however, advancement of the research in this work depends on the pursuit of a true steam reforming mechanism over rhodium or nickel instead of the adaptation of a mechanism designed for partial oxidation. Particular attention should be placed on the adsorption of CH_4 and H_2O and the desorption of CO as they tend to control the activity of the catalyst. Apart from mechanism development, washcoat effectiveness needs to be included, particularly when the channel diameter is reduced making the spatial variation within the washcoat more significant.

References

Ahmed, S. and M. Krumpelt (2001). "Hydrogen from hydrocarbon fuels for fuel cells." International Journal of Hydrogen Energy **26**(4): 291-301.

Balasubramanian, B., A. L. Ortiz, et al. (1999). "Hydrogen from methane in a single-step process." Chemical Engineering Science **54**(15-16): 3543-3552.

Brown, L. F. (2001). "A comparative study of fuels for on-board hydrogen production for fuel-cell-powered automobiles." International Journal of Hydrogen Energy **26**(4): 381-397.

Burch, R. and F. J. Urbano (1995). "Investigation of the active state of supported palladium catalysts in the combustion of methane." Applied Catalysis A: General **124**: 121-138.

Coltrin, M. E., R. J. Kee, et al. (1996). SURFACE CHEMKIN-III: a FORTRAN package for analyzing heterogeneous chemical kinetics at a solid-surface gas-phase interface, Sandia National Lab Report SAND96-8217.

Deuflhard, P., E. Hairer, et al. (1987). "One-step and extrapolation methods for differential-algebraic systems." Numer. Math. **51**: 501-516.

Deutschmann, O. and L. D. Schmidt (1998). "Modeling the partial oxidation of methane in a short-contact- time reactor." Aiche Journal **44**(11): 2465-2477.

Fant, D., G. S. Jackson, et al. (2000). "Status of catalytic combustion R&D for the Department of Energy Advanced Turbine Systems Program." Journal of Engineering for Gas Turbines and Power-Transactions of the Asme **122**(2): 293-300.

Farrauto, R. J., M. C. Hobson, et al. (1992). "Catalytic chemistry of supported palladium for combustion of methane." Applied Catalysis A: General **81**: 227-237.

Forzatti, P. and G. Groppi (1999). "Catalytic combustion for the production of energy." Catalysis Today **54**: 165-180.

Frauhammer, J., G. Eigenberger, et al. (1999). "A new reactor concept for endothermic high-temperature reactions." Chemical Engineering Science **54**(15-16): 3661-3670.

Freni, S., G. Calogero, et al. (2000). "Hydrogen production from methane through catalytic partial oxidation reactions." Journal of Power Sources **87**(1-2): 28-38.

Fujimoto, K., F. H. Ribeiro, et al. (1998). "Structure and reactivity of PdO_x/ZrO_2 catalysts for methane oxidation at low temperatures." Journal of Catalysis **179**: 431-442.

G. Groppi, M. V., P. Forzatti (2001). Chemical Engineering Science **56**: 831.

Gelin, P. and M. Primet (2002). "Complete oxidation of methane at low temperature over noble metal based catalysts: a review." Applied Catalysis B: Environmental **39**: 1-37.

Groppi, G., A. Belloli, et al. (1995). "A comparison of lumped and distributed models of monolith catalytic combustors." Chemical Engineering Science **50**: 2705-2715.

Han, J., I. Kim, et al. (2000). "Purifier-integrated methanol reformer for fuel cell vehicles." Journal of Power Sources **86**: 223-227.

Harvey, S. P. and H. J. Richter (1994). "Gas turbine cycles with solid oxide fuel cells. Part II: A detailed study of a gas turbine cycle with an integrated internal reforming solid oxide fuel cell." Journal of Energy Resources Technology **116**: 312-318.

Hegedus, L. L. (1975). "Temperature excursions in catalytic monoliths." Aiche Journal **21**: 849-853.

Heinzel, A. (2002). "Reforming of natural gas - hydrogen generation for small scale stationary fuel cell systems." Journal of Power Sources **105**: 202-207.

Hickman, D. A. and L. D. Schmidt (1993). "Steps in Ch_4 oxidation on Pt and Rh surfaces - high-temperature reactor simulations." Aiche Journal **39**(7): 1164-1177.

Hou, K. H. and R. Hughes (2001). "The kinetics of methane steam reforming over a Ni/α-Al_2O_3 catalyst." Chemical Engineering Journal **82**(1-3): 311-328.

Kolios, G., J. Frauhammer, G. Eigenberger (2002). "Efficient reactor concepts for coupling of endothermic and exothermic reactions." Chemical Engineering Science **57**: 1505-1510.

Kramer, J. F., S. S. Reihani, et al. (2003). "Low temperature combustion of hydrogen on supported Pd catalysts". Combustion Institute, 29, 989-996.

Krumpelt, M., T. R. Krause, et al. (2002). "Fuel processing for fuel cell systems in transportation and portable power applications." Catalysis Today **77**: 3-16.

Lyubovsky, M. and L. Pfefferle (1998). "Methane combustion over the α-alumina supported Pd catalyst: Activity of the mixed Pd/PdO state." Applied Catalysis A: General **173**: 107-119.

Lyubovsky, M. and L. Pfefferle (1999). "Complete methane oxidation over Pd catalyst supported on α-alumina. Influence of temperature and oxygen pressure on the catalyst." Catalysis Today **47**: 29-44.

McCarty, J. G. and Y.-f. Chang (1994). "Dispersion of palladium on alumina surfaces." Scripta Metallurgica et Materialia **31**(8): 1115.

Palsson, J., A. Selimovic, et al. (2000). "Combined solid oxide fuel cell and gas turbine systems for efficient power and heat generation." Journal of Power Sources **86**(1-2): 442-448.

Reihani, S. and G. Jackson (2004). "Effectivenss in catalytic washcoats with multi-step mechanisms for catalytic combustion of hydrogen." in press, Chemical Engineering Science.

Rosen, M. A. (1991). "Thermodynamic Investigation of Hydrogen-Production by Steam Methane Reforming." International Journal of Hydrogen Energy **16**(3): 207-217.

Rostrup-Nielsen, J. R. (1984). Catalytic Steam Reforming. New York, Springer-Verlag.

Rostrup-Nielsen, J. R. and D. L. Trimm (1977). "Mechanisms of carbon formation on nickel-containing catalysis." Journal of Catalysis **48**: 155-165.

Schwiedernoch, R., S. Tischer, et al. (2003). "Experimental and numerical study on the transient behavior of partial oxidation of methane in a catalytic monolith." Chemical Engineering Science **58**: 633-642.

Trimm, D. L. (1999). "Catalysts for the control of coking during steam reforming." Catalysis Today **49**: 3-10.

Trimm, D. L. and Z. I. Onsan (2001). "Onboard fuel conversion for hydrogen-fuel-cell-driven vehicles." Catalysis Reviews **43 (1&2)**: 31-84.

Turns, S. R. (2000). An Introduction to Combustion: Concepts and Applications. Boston, McGraw Hill.

Wolf, M., H. Zhu, et al. (2003). "Kinetic model for polycrystalline Pd/PdO_x in oxidation/reduction cycles." Applied Catalysis A: General **244**(2): 323-340.

Xu, J. G. and G. F. Froment (1989). "Methane Steam Reforming, Methanation and Water-Gas Shift .1. Intrinsic Kinetics." Aiche Journal **35**(1): 88-96.

Zhu, H. (2001). Numerical modeling of methane combustion on palladium catalyst for gas turbine applications. Mechanical Engineering. College Park, University of Maryland at College Park.

Zhu, J., D. Zhang, et al. (2001). "Reforming of CH4 by partial oxidation: thermodynamic and kinetic analyses." Fuel **80**(7): 899-905.